SCATTERING AND RADIATION PROBLEMS OF ARBITRARILY SHAPED CONDUCTING BODIES ABOVE THE GROUND PLANE

A THESIS

SUBMITTED TO THE DEPARTMENT OF ELECTRICAL AND

ELECTRONICS ENGINEERING

AND THE INSTITUTE OF ENGINEERING AND SCIENCES

OF BILKENT UNIVERSITY

IN PARTIAL FULFILLMENT OF THE REQUIREMENTS

FOR THE DEGREE OF

MASTER OF SCIENCE

By

Cemal C. Yıldırım

October 2002

I certify that I have read this thesis and that in my opinion it is fully adequate, in scope and in quality, as a thesis for the degree of Master of Science.

_____

Assoc. Prof. Dr. Levent Gürel (Supervisor)

I certify that I have read this thesis and that in my opinion it is fully adequate, in scope and in quality, as a thesis for the degree of Master of Science.

_____

Prof. Dr. Yusuf Ziya İder

I certify that I have read this thesis and that in my opinion it is fully adequate, in scope and in quality, as a thesis for the degree of Master of Science.

_____

Asst. Prof. Dr. Vakur B. Ertürk

Approved for the Institute of Engineering and Sciences:

_____

Prof. Dr. Mehmet Baray
Director of Institute of Engineering and Sciences

ii

ABSTRACT

SCATTERING AND RADIATION PROBLEMS OF ARBITRARILY SHAPED CONDUCTING BODIES ABOVE THE GROUND PLANE

Cemal C. Yıldırım

M.S. in Electrical and Electronics Engineering

Supervisor: Assoc. Prof. Dr. Levent Gürel

October 2002

A method of moment solution is applied for the scattering and radiation problems of arbitrarily shaped conducting bodies placed close to an infinite ground plane. An equivalent problem is produced by using image theory and solved by two methods. Free-space Green's function is used for the first method, and modified free-space Green's function is used for the second. The conducting bodies excited with either an incident plane-wave or a delta-gap source. Moreover, the definition method of the basis functions is explained when multiple unknowns occur at a single edge.

Keywords: Method of moments, image theory, radar cross section (RCS), delta-gap source.

ÖZET

SONSUZ İLETKEN DÜZLEM ORTAMINDA GELİŞİGÜZEL ŞEKİLLİ İLETKEN CİSİMLERİN SAÇINIM VE IŞINIM PROBLEMLERİ

Cemal C. Yıldırım

Elektrik ve Elektronik Mühendisliği Bölümü Yüksek Lisans

Tez Yöneticisi: Doç. Dr. Levent Gürel

Ekim 2002

Sonsuz iletken düzlem üzerinde bulunan gelişigüzel şekilli iletken cisimlerin elektromanyetik saçınım karasteriklerini belirlemek için momentler metodu kullanılmıştır. İletken düzlem imaj teorisi kullanılarak kaldırılmış ve eşdeğer problem üretilmiştir. Eşdeğer problem iki yöntemle çözülmüştür. İlk yöntemde serbest uzay Green fonksiyonu, ikincisinde cismin yüzeyinde indüklenmiş gerçek ve kurgusal akımların arasındaki eşitlik kullanılarak değiştirilen Green fonksiyonu kullanılmıştır. Saçınım çözümlerinde gelen düzlem dalga, ışınım çözümlerinde voltaj beslemesi kaynak olarak kullanılmıştır. Ayrıca gelişigüzel yüzeyli cisimlerin üçgenlenmesi sonrasında ikiden fazla üçgenin bağlı olduğu kenarlarda temel fonksiyonların nasıl tanımlanacağı açıklanmıştır.

Anahtar kelimeler: Momentler metodu, imaj teorisi, radar kesit alanı (RKA).

ACKNOWLEDGMENTS

I gratefully thank my supervisor Dr. Levent Gürel for his supervision, guidance, and suggestions throughout the development of this thesis.

Contents

List of Figures

List of Tables

To My Family . . .

Chapter 1

Introduction

The prediction and reduction of radar cross section (RCS) of arbitrary shapes is one of the most popular topics for researchers in electromagnetics. From the military requirements aspect, these studies are carried out to design stealthy objects or to reduce the RCS of existing targets by using radar absorbing materials (RAMs). Upon successful construction of low-observable aircrafts, similar studies are initiated for warships. However, the problems encountered during these studies have become more challenging due to the large bodies of ships and the effects of sea surface.

RCS reduction techniques are generally classified as body shaping, using RAMs, and active/passive cancellation. In most applications, the transmitter and receiver of radars are on the same location which is called as monostatic radars. Therefore the term "RCS reduction" can be considered as reduction of monostatic RCS. Body shaping is based on to steer the electromagnetic energy from the scatterer to directions excluding the direction of incident energy. Especially at frequencies which scattering property of a typical target approximates the quasi-optical character, shaping becomes the most important key to reduce

the monostatic RCS. In order to prevent backscattering, all smooth elements on the target which are perpendicular to the direction of incident electromagnetic energy must be removed [1]. Furthermore, numerical analysis of such problems is carried out by using asymptotic methods like physical optics (PO), physical theory of diffraction (PTD), geometrical optics (GO), and general theory of diffracted rays (GTD).

Coating RAMs on the surface of the target is another technique used for the reduction of not only monostatic but also bistatic RCS. The term "bistatic" expresses that the locations of transmitter and receiver of a radar are different. RAMs transforms electromagnetic energy into heat and is categorized as materials with electric losses and materials with magnetic losses.

In order to computationally solve electrically large problems, new techniques have been developed, such as the multi-level fast multipole algorithm (MLFMA), shooting and bouncing ray (SBR) method, and hybridization of different methods. Modeling the sea surface is another computational requirement. An infinite ground plane can be considered as the very basic model of the sea surface.

In this thesis, a method of moment (MoM) solution is applied for the scattering and radiation problems of arbitrarily shaped conducting bodies above an infinite ground plane. Method of moments is a well-known technique used to solve integral equations by reducing the integral equation to a set of linearly independent equations [2]. This method requires the discretization of the surface. In our numerical solutions, the surfaces are meshed with triangles, since the basis functions used to expand the induced currents are defined on triangle pairs.

The image theory is used to take the effect of the ground plane into account, and an equivalent problem is formed. In Chapters 2 and 3, two different formulations of the problem are carried out by considering whether the conducting body is touching the ground plane or not. Furthermore, two different excitation types

are employed: scattering problems involve incident plane-wave excitation, and radiation problems involve delta-gap source excitation. Different applications of delta-gap sources are illustrated in Chapter 4.

Finally, the difficulties emerging from the definition of basis functions for complex geometries are considered. The MoM relies on the properly defined basis functions to expand the induced currents on the surface of the body. Complex bodies involve multiple structures joining at the same edge. Chapter 5 provides detailed explanations for the definition of the basis functions for these types of edges.

Chapter 2

Scattering from a Conducting Body above an Infinite Ground Plane

In order to solve the scattering problem of a conducting body in the presence of an infinite ground plane, the method of images [3] is used to obtain an equivalent problem. Then, we can solve the problem numerically by using the method of moments [2]. Figure 2.1 demonstrates the original and the equivalent problems. In the original problem, a conducting body with an arbitrary shape is illuminated by an external source. Therefore, we take into account the images of both the conducting body and the external source. There are two approaches to solve the equivalent problem. One of them is to solve the problem by applying the free-space Green's function after employing the method of images explicitly. The second one is to solve the problem by applying a modified free-space Green's function, which is derived by using the properties of method of images inherently,

but not explicitly. We use both of the methods in our numerical solutions and compare the results.
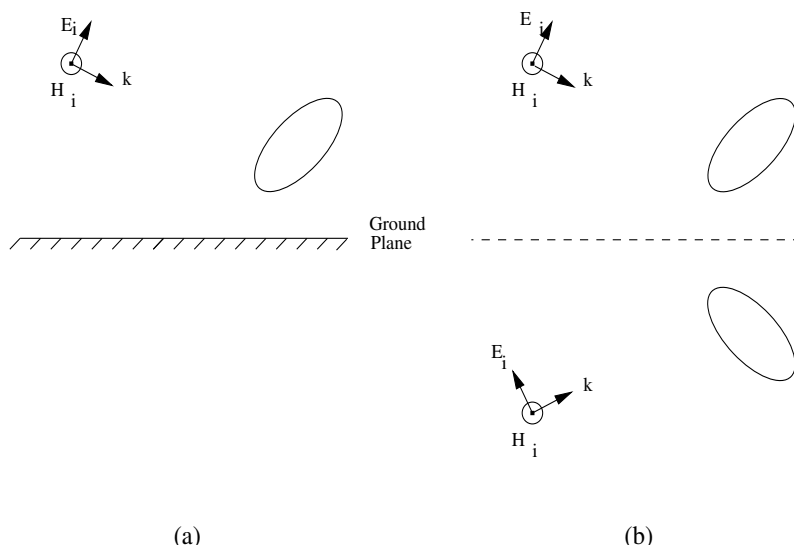
Figure 2.1: (a) A conducting body over a ground plane illuminated by an electromagnetic source. (b) The equivalent problem.

2.1 An Overview of the Method of Moments (MoM)

Method of moments (MoM) [2] transforms linear integral equations to linear algebraic equations. Radiation and scattering problems can be formulated in terms of integral equations, and discretized for numerical solutions. By using MoM, the electric field integral equation (EFIE) can be reduced to a matrix equation. We use Rao, Wilton, and Glisson (RWG) basis functions [4] for the discretization of the EFIE.

2.2   Formulation of the Scattering Problem

The induced current $\mathbf{J}(\mathbf{r}')$ on the surface of conducting body can be represented as a group of small dipoles with arbitrary directions. Assume that we have a rectangular plate above the ground plane at $z = 0$. Figure 2.2 shows some of the samples of induced currents over the triangulated surface of a rectangular plate in terms of electric dipoles and the equivalent problem. After this step, formulation of the problem can be carried out by considering the relation between the real and image dipoles.

Original   Problem :

Equivalent   Problem :
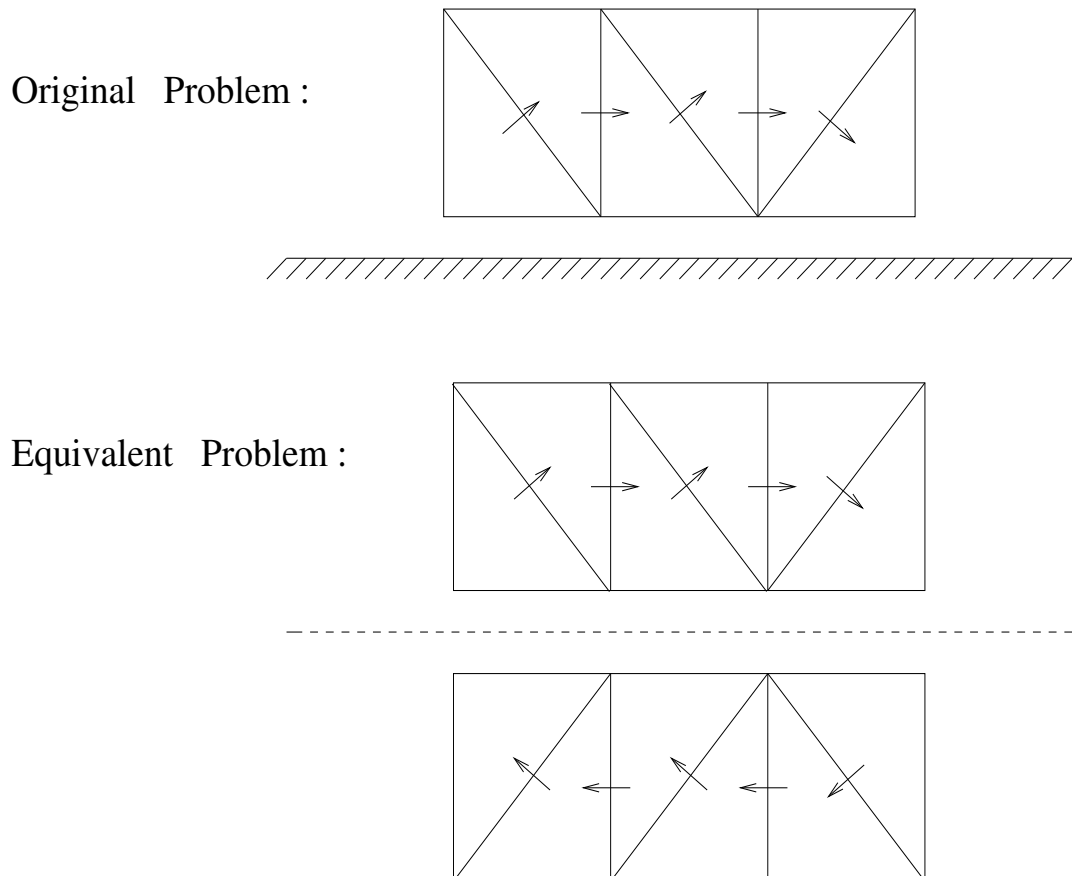
Figure 2.2: Samples of induced currents on the triangulated surface of the rectangular plate above the ground plane and the equivalent problem.

According to the method of images, real and image electric dipoles are equal to each other in terms of magnitude,their parallel components are in opposite

directions, and their normal components are in the same direction, as shown in Figure 2.3.

Original Problem :

Equivalent Problem :
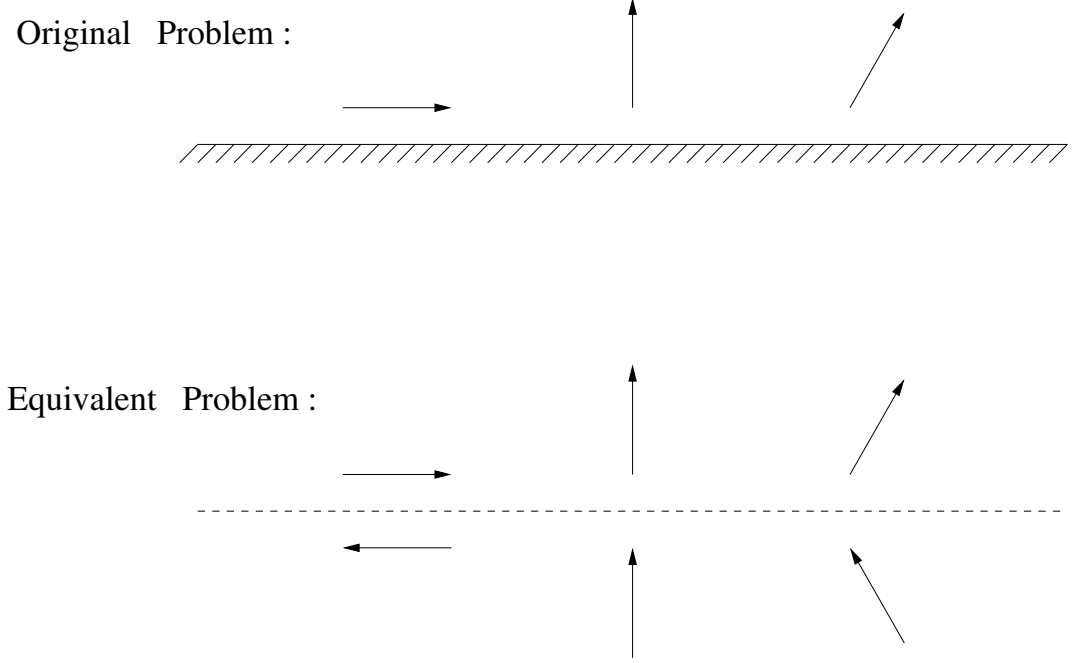
Figure 2.3: The relation between the real and image electric dipoles.

We can define the induced current on the surface of conducting body in Figure 2.1 in terms of real and image currents by using the equivalent problem:

$$\mathbf{J}^{tot}(\mathbf{r'}) = \mathbf{J}^{real}(\mathbf{r'}) + \mathbf{J}^{image}(\mathbf{r'}). \qquad (2.1)$$

Assume that the ground plane is at $z = 0$, and we have an electric dipole at point p (x_p, y_p, z_p):

$$\mathbf{J}^{real}(\mathbf{r'}) = \delta(x' - x_p)\delta(y' - y_p)\delta(z' - z_p)\{\hat{x}J_x + \hat{y}J_y + \hat{z}J_z\},$$
$$\mathbf{J}^{image}(\mathbf{r'}) = \delta(x' - x_p)\delta(y' - y_p)\delta(z' + z_p)\{-\hat{x}J_x - \hat{y}J_y + \hat{z}J_z\}. \qquad (2.2)$$

In Eq. (2.2), J_x, J_y, and J_z are the magnitudes of the electric dipole. We can express the scattered field as follows:

$$\mathbf{E}^{scat}(\mathbf{r}) = iw\mu\left[\bar{\mathbf{I}} + \frac{1}{k^2}\nabla\nabla\right] \cdot \int_{s'} ds' g(\mathbf{r}, \mathbf{r'})\mathbf{J}^{tot}(\mathbf{r'}). \qquad (2.3)$$

We can rewrite the integrand of the inner integral in Eq. (2.3) by using the definitions in Eq. (2.2):

$$
\begin{aligned}
\mathbf{J}^{tot}(\mathbf{r}')g(\mathbf{r},\mathbf{r}') &= \delta(x'-x_p)\delta(y'-y_p)\delta(z'-z_p)\{\hat{x}J_x+\hat{y}J_y+\hat{z}J_z\}g(\mathbf{r},\mathbf{r}') \\
&+ \delta(x'-x_p)\delta(y'-y_p)\delta(z'+z_p)\{-\hat{x}J_x-\hat{y}J_y+\hat{z}J_z\}g(\mathbf{r},\mathbf{r}') \\
\\
&= \{\hat{x}J_x+\hat{y}J_y+\hat{z}J_z\}\frac{e^{ik\sqrt{(x-x_p)^2+(y-y_p)^2+(z-z_p)^2}}}{4\pi\sqrt{(x-x_p)^2+(y-y_p)^2+(z-z_p)^2}} \\
&+ \{-\hat{x}J_x-\hat{y}J_y+\hat{z}J_z\}\frac{e^{ik\sqrt{(x-x_p)^2+(y-y_p)^2+(z+z_p)^2}}}{4\pi\sqrt{(x-x_p)^2+(y-y_p)^2+(z+z_p)^2}}.
\end{aligned}
$$
$$(2.4)$$

Since the primed coordinates are used for the source (induced currents on the surface), we can replace (x_p,y_p,z_p) with (x',y',z').

$$
\begin{aligned}
\mathbf{J}^{tot}(\mathbf{r}')g(\mathbf{r},\mathbf{r}') &= \{\hat{x}J_x+\hat{y}J_y+\hat{z}J_z\}\underbrace{\frac{e^{ik\sqrt{(x-x')^2+(y-y')^2+(z-z')^2}}}{4\pi\sqrt{(x-x')^2+(y-y')^2+(z-z')^2}}}_{g_{real}(\mathbf{r},\mathbf{r}')} \\
&+ \{-\hat{x}J_x-\hat{y}J_y+\hat{z}J_z\}\underbrace{\frac{e^{ik\sqrt{(x-x')^2+(y-y')^2+(z+z')^2}}}{4\pi\sqrt{(x-x')^2+(y-y')^2+(z+z')^2}}}_{g_{image}(\mathbf{r},\mathbf{r}')},
\end{aligned}
$$
$$(2.5)$$

After simple manipulations, we obtain

$$
\begin{aligned}
\bar{\bar{G}}_{GP}(\mathbf{r},\mathbf{r}')\cdot\mathbf{J}(\mathbf{r}') &= (\hat{x}J_x+\hat{y}J_y)\{g_{real}(\mathbf{r},\mathbf{r}')-g_{image}(\mathbf{r},\mathbf{r}')\} \\
&+ \hat{z}J_z\{g_{real}(\mathbf{r},\mathbf{r}')+g_{image}(\mathbf{r},\mathbf{r}')\}.
\end{aligned}
$$
$$(2.6)$$

The matrix form of modified Green's function defined in Eq. (2.6) is as follows:

$$
\bar{\bar{G}}_{GP}(\mathbf{r},\mathbf{r}') = \begin{bmatrix} g_{real}(\mathbf{r},\mathbf{r}')-g_{image}(\mathbf{r},\mathbf{r}') & 0 & 0 \\ \\ 0 & g_{real}(\mathbf{r},\mathbf{r}')-g_{image}(\mathbf{r},\mathbf{r}') & 0 \\ \\ 0 & 0 & g_{real}(\mathbf{r},\mathbf{r}')+g_{image}(\mathbf{r},\mathbf{r}') \end{bmatrix}. \quad (2.7)
$$

Eq. (2.6) is the integrand of the inner integral of Eq. (2.3). Thus, we can obtain the scattered field produced by the induced currents on the surface of a conducting body above a ground plane. By using boundary condition on the surface of conducting body ($\mathbf{E}_{tan}^{tot} = \mathbf{E}_{tan}^{scat} + \mathbf{E}_{tan}^{inc} = 0$), we can relate the incident field to the induced current as

$$\hat{t} \cdot \mathbf{E}_{tot}^{inc} = -\hat{t} \cdot iw\mu \left[\bar{\bar{\mathbf{I}}} + \tfrac{1}{k^2}\nabla\nabla \right] \cdot \int_{s'} ds' \bar{\bar{G}}_{GP}(\mathbf{r},\mathbf{r}') \cdot \mathbf{J}(\mathbf{r}'), \tag{2.8}$$

which is the EFIE, where $\hat{t}$ is one of the two tangential directions on the surface and

$$\mathbf{E}_{tot}^{inc} = \mathbf{E}_{real}^{inc} + \mathbf{E}_{image}^{inc}. \tag{2.9}$$

In Eq. (2.8), we know the incident field, and try to determine the induced currents. In order to solve for the induced currents, this integral equation is reduced to a matrix equation by using the method of moments. For this purpose, the induced currents are expanded in terms of the RWG vector basis functions:

$$\bar{\bar{G}}_{GP}(\mathbf{r},\mathbf{r}') \cdot \mathbf{J}(\mathbf{r}') = \sum_{j=1}^{N} \alpha_j \Big[(\hat{x}b_{jx} \quad + \quad \hat{y}b_{jy})\{g_{real}(\mathbf{r},\mathbf{r}') - g_{image}(\mathbf{r},\mathbf{r}')\}$$

$$+ \quad \hat{z}b_{jz}\{g_{real}(\mathbf{r},\mathbf{r}') + g_{image}(\mathbf{r},\mathbf{r}')\} \Big]$$

$$= \sum_{j=1}^{N} \alpha_j \bar{\bar{G}}_{GP}(\mathbf{r},\mathbf{r}') \cdot \mathbf{b}_j(\mathbf{r}') \tag{2.10}$$

The resulting equation is given by

$$\hat{t} \cdot \mathbf{E}_{tot}^{inc} = -\hat{t} \cdot iw\mu \left[\bar{\bar{\mathbf{I}}} + \tfrac{1}{k^2}\nabla\nabla \right] \cdot \int_{s'} ds' \bar{\bar{G}}_{GP}(\mathbf{r},\mathbf{r}') \cdot \sum_{j=1}^{N} \alpha_j \mathbf{b}_j(\mathbf{r}'). \tag{2.11}$$

The above EFIE is tested by the testing functions $\mathbf{t}_i(\mathbf{r})$, which are chosen to be the same as the basis functions:

$$\underbrace{-\int_s ds\, \mathbf{t}_i(\mathbf{r}) \cdot \mathbf{E}_{tot}^{inc}}_{V_i} = \sum_{j=1}^{N} \alpha_j \underbrace{\int_s ds\, \mathbf{t}_i(\mathbf{r}) \cdot iw\mu \left[\bar{\bar{\mathbf{I}}} + \tfrac{1}{k^2}\nabla\nabla \right] \cdot \int_{s'} ds' \bar{\bar{G}}_{GP}(\mathbf{r},\mathbf{r}') \cdot \mathbf{b}_j(\mathbf{r}')}_{Z_{ij}}$$

$$\tag{2.12}$$

Consequently, we obtain N equations, where N is equal to the number of basis and testing functions. In these equations, the unknowns are the coefficients of the basis functions (α_j). Then, we have N linearly independent equations for N unknowns. Matrix form of these equations is given by

$$
\begin{bmatrix}
Z_{11} & Z_{12} & \dots & Z_{1N} \\
Z_{21} & Z_{22} & \dots & Z_{2N} \\
\vdots & \vdots & \ddots & \vdots \\
Z_{N1} & Z_{N2} & \dots & Z_{NN}
\end{bmatrix}
\cdot
\begin{bmatrix}
\alpha_1 \\
\alpha_2 \\
\vdots \\
\alpha_N
\end{bmatrix}
=
\begin{bmatrix}
V_1 \\
V_2 \\
\vdots \\
V_N
\end{bmatrix}
\tag{2.13}
$$

The matrix is called the impedance matrix. If we use the free-space Green's function for the solution of the equivalent problem, we will obtain a similar matrix of size $2N \times 2N$.

2.3 Examples

For the examples considered here, the monostatic RCS results obtained by two different methods are compared. These two methods are as follows:

1. Method 1: By defining the images of the actual basis functions, number of unknowns is doubled and the free-space Green's function is employed.

2. Method 2: Image theory is used to derive a modified Green's function for the infinite ground plane. In this case, the number of unknowns is not doubled.

Figures 2.4 and 2.5 present the geometry of a conducting cube whose dimensions are $0.3 \times 0.3 \times 0.3$ meters above the ground plane, and its RCS results obtained with the two different solution methods. Similarly, Figures 2.6 and 2.7

show the geometry and results of a conducting cylinder whose dimensions are $h = 1$ m and $r = 0.1$ m. In the first problem, the numbers of unknowns for the first and the second methods are 504 and 1008, respectively. In the second one, the numbers of unknowns are 951 and 1902.

In both problems, the objects are illuminated with a y-polarized plane wave. The incidence angle of the field measured from x-axis in the x-z plane is varying between 0°-180° with 5° intervals. Since the left hand side (LHS) of Eq. (2.12) depends on the incidence angle, 37 different matrix equations are solved. RCS plots of conducting bodies are calculated in three different planes (xy, xz, and yz). In order to compute the monostatic RCS results, the direction of scattering is chosen to be the exactly opposite of the direction of incidence. Since the results are consistent with each other, we can conclude that the formulation of the second method is correct.
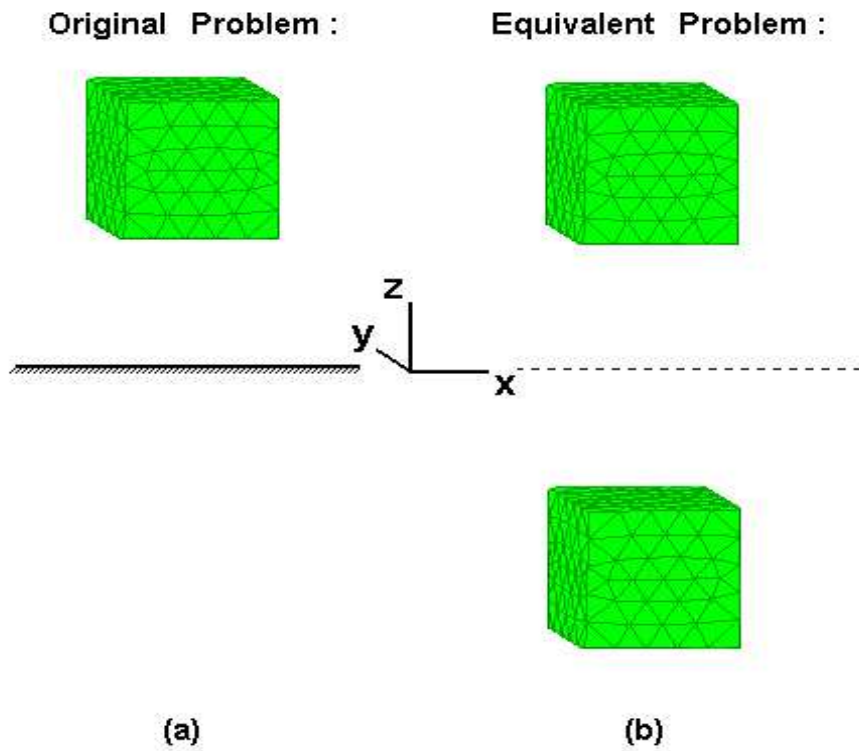
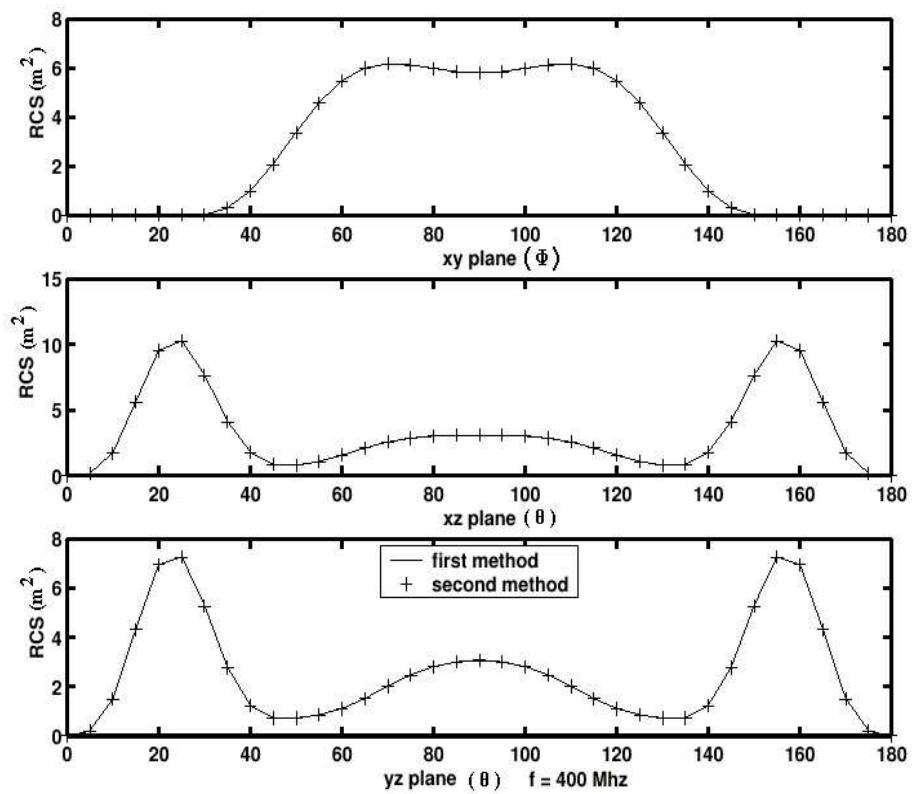Figure 2.4: (a) A conducting cube above the ground plane. (b) The equivalent problem.

Figure 2.5: The monostatic RCS results of the cube shown in Figure 2.4 (a).

12
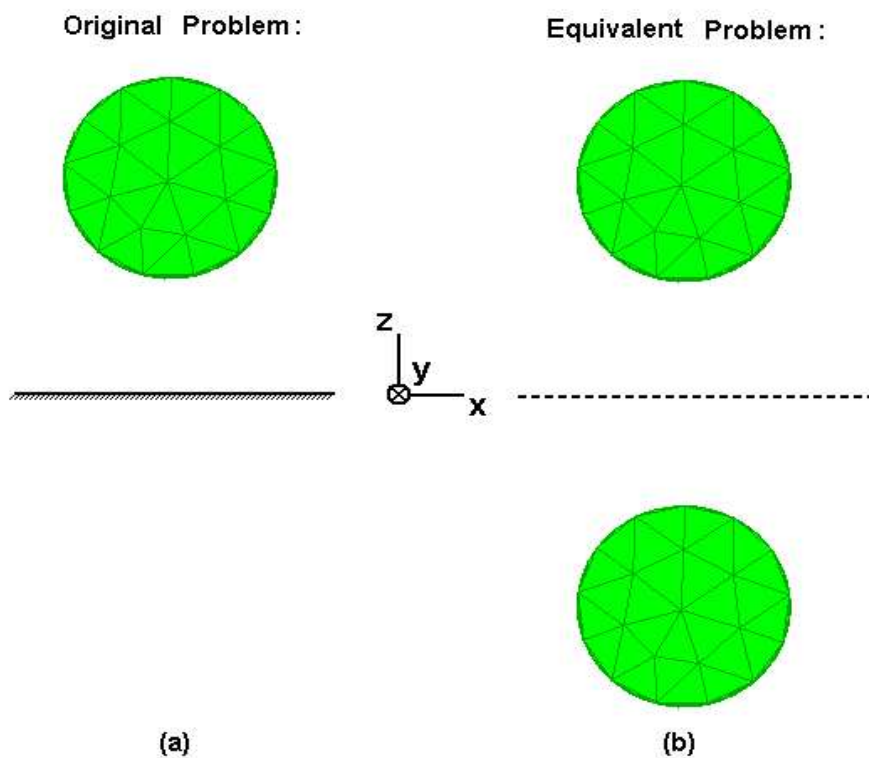
Figure 2.6: (a) A conducting cylinder above the ground plane. (b) The equivalent problem.
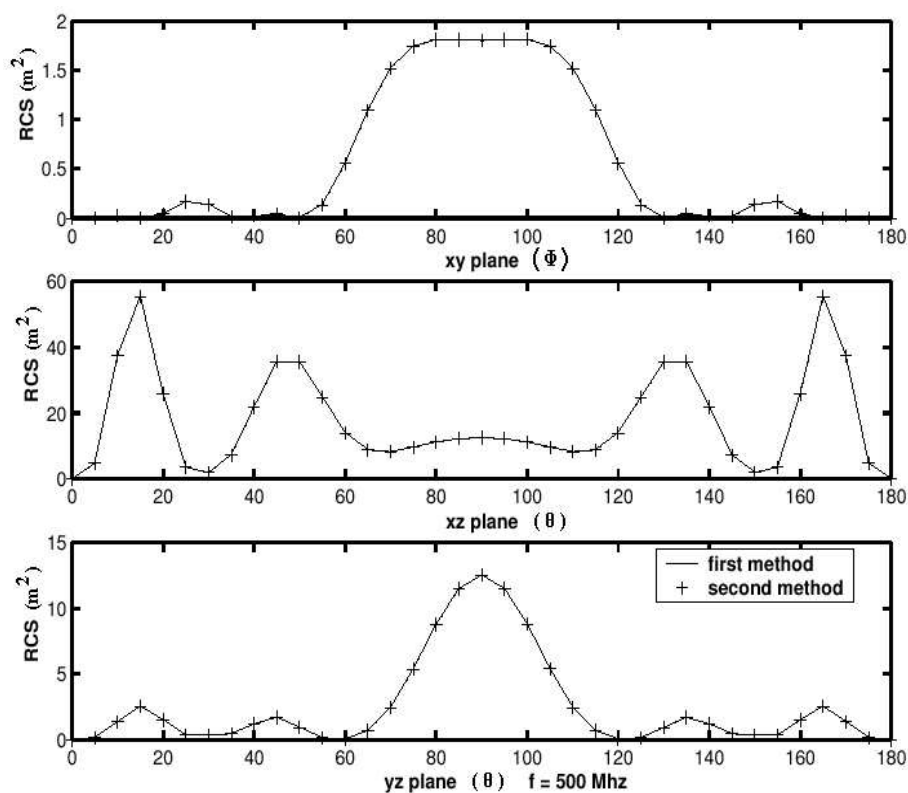
Figure 2.7: The monostatic RCS results of the cylinder shown in Figure 2.6 (a).

Chapter 3

Scattering from a Conducting Body Touching the Ground Plane

In Chapter 2, a formulation of the scattering problem of a conducting body in the presence of a ground plane is derived by assuming that the conducting body does not touch the ground plane. Figure 3.1 shows the original and equivalent problems when the body touches the ground plane. Since the conducting body is touching its image at the level of the ground plane, the induced current should be able to flow among real and image triangles. The formulation derived for the scattering problem in Chapter 2 remains the same with the exception of definition of new basis functions on the triangles touching the ground plane. In addition to the regular basis functions on adjacent triangles (on common edges where triangles are connected), new basis functions should be defined on those triangles, whose one of the edges is on the ground plane. Since RWG vector basis functions are defined on triangle pairs [4], it is not possible to directly use them

on single boundary triangles. If we try to reformulate the RWG basis functions on single triangles, we will be confronted with non-integrable singularities on the edges of the triangles. However, modifying the triangulated surface as shown in Figure 3.2 enables new basis functions to be defined on boundary triangles.

(a)

(b)
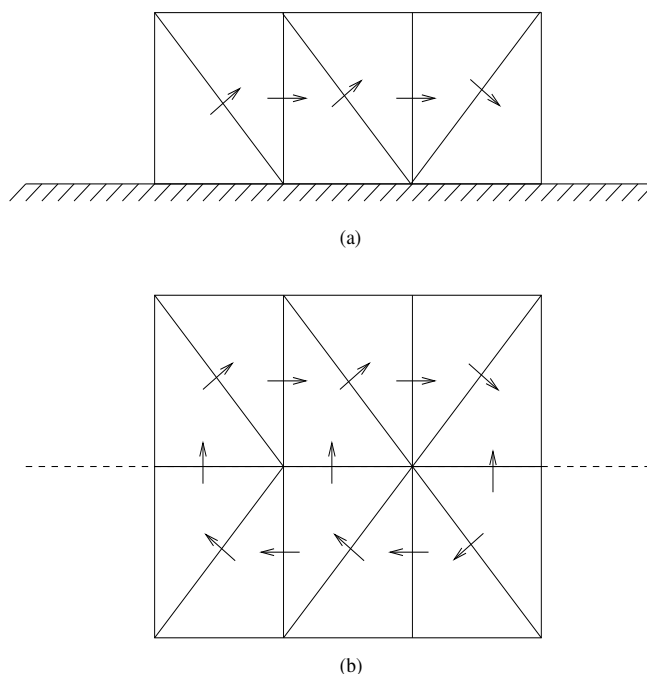
Figure 3.1: (a) A conducting rectangular plate touching the ground plane. (b) The equivalent problem.
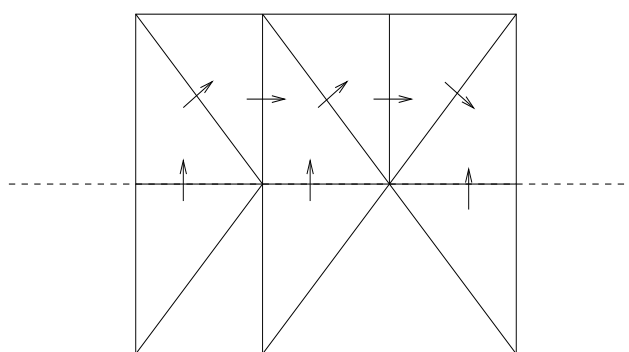
Figure 3.2: Modified triangulated surface of the rectangular plate.

3.1 Reformulating RWG Basis Functions

In this section, we examine the pitfalls of the formulation when we try to construct an RWG basis function (BF) on a single triangle. Figure 3.3 depicts an RWG BF on a triangle pair, which is defined as
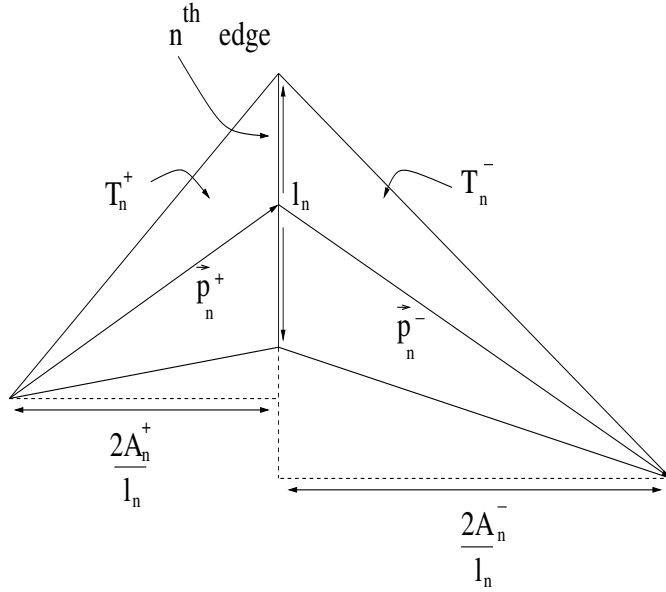
Figure 3.3: Definition of an RWG basis function on adjacent triangles.

$$
\mathbf{f}_n(\mathbf{r}') = \begin{cases} \frac{\ell_n}{2A_n^+}\rho_{\mathbf{n}}^+ & \mathbf{r}' \in T_n^+, \\ \frac{\ell_n}{2A_n^-}\rho_{\mathbf{n}}^- & \mathbf{r}' \in T_n^-, \\ 0 & \text{otherwise.} \end{cases} \tag{3.1}
$$

We use a shape function $S(\mathbf{r}')$ in order to bound basis function on one triangle:

$$
\mathbf{f}_n(\mathbf{r}')S(\mathbf{r}') = \begin{cases} \frac{\ell_n}{2A_n^+}\rho_{\mathbf{n}}^+ & \mathbf{r}' \in T_n^+, \\ 0 & \text{otherwise,} \end{cases} \tag{3.2}
$$

where

$$
S(\mathbf{r}') = \begin{cases} 1 & \mathbf{r}' \in T_n^+, \\ 0 & \text{otherwise.} \end{cases} \tag{3.3}
$$

While transforming the EFIE (2.8) to a matrix equation, we need to take the divergence of basis (testing) functions. Due to the shape function's discontinuity

on edges, divergence of Eq. (3.2) produces delta functions:

$$\nabla' \cdot \left[\mathbf{f}_n(\mathbf{r}')S(\mathbf{r}')\right] = \frac{\ell_n}{A_n^+}S(\mathbf{r}') - \hat{n}' \cdot \mathbf{f}_n(\mathbf{r}')\delta(\mathbf{r}' - \mathbf{r}_{\ell_n}). \qquad (3.4)$$

In the EFIE, these delta functions convert some surface integrals to line integrals. By substituting the second term of Eq. (3.4), the following expression is obtained:

$$\int_{s'} ds' \left[- \hat{n}' \cdot \mathbf{f}_n(\mathbf{r}')\delta(\mathbf{r}' - \mathbf{r}_{\ell_n})\right] g(\mathbf{r}, \mathbf{r}') = - \int_{\ell_n'} d\ell' \hat{n}' \cdot \mathbf{f}_n(\mathbf{r}')\frac{e^{ik|\mathbf{r} - \mathbf{r}'|}}{|\mathbf{r} - \mathbf{r}'|}. \qquad (3.5)$$

Numerical computation of the above integral on adjacent and self triangles requires the extraction and analytical evaluation of the singularity:

$$\int_{\ell_n'} d\ell' \hat{n}' \cdot \mathbf{f}_n(\mathbf{r}')\frac{e^{ik|\mathbf{r} - \mathbf{r}'|}}{|\mathbf{r} - \mathbf{r}'|} = \int_{\ell_n'} d\ell' \hat{n}' \cdot \mathbf{f}_n(\mathbf{r}')\frac{(e^{ik|\mathbf{r} - \mathbf{r}'|} - 1)}{|\mathbf{r} - \mathbf{r}'|} + \int_{\ell_n'} d\ell' \hat{n}' \cdot \mathbf{f}_n(\mathbf{r}')\frac{1}{|\mathbf{r} - \mathbf{r}'|}.$$
$$(3.6)$$

Although the integration of $1/|\mathbf{r} - \mathbf{r}'|$ is achievable on a surface [5]-[6], it is not possible to analytically integrate the same singularity on a line. Therefore, we cannot use the reformulated basis function (3.2) in order to discretize the EFIE.

3.2   Modifying the Triangulated Surface

Firstly, the intersection area between the body and the ground plane should be removed due to the fact that the tangential electric currents on the ground plane do not radiate. Then, we obtain modified triangulated surface of the body by taking images of the boundary triangles. Thus, new basis functions can be defined on edges where sawtooth-style triangles are connected. Figure 3.4(a), (b) and (c) show the steps of modifying a conducting cube.
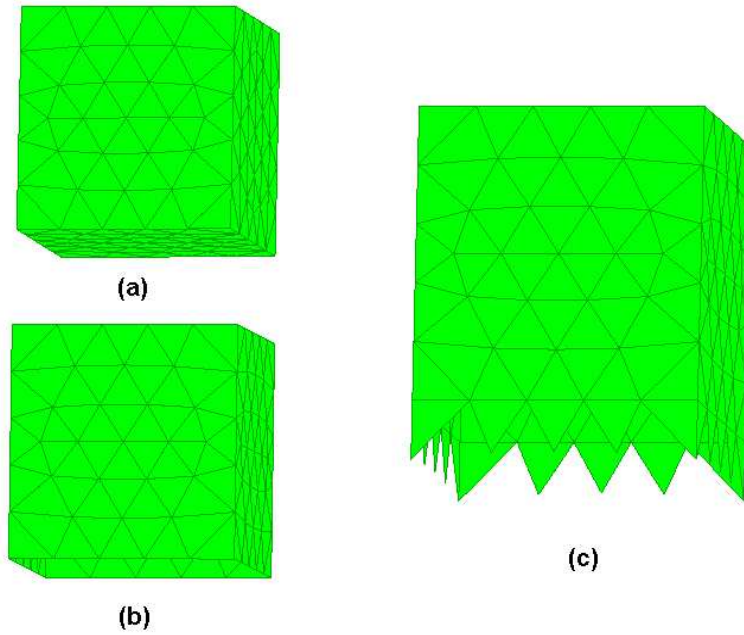
Figure 3.4: (a) A conducting cube. (b) The same conducting cube with an open side. (c) Modified form of the conducting cube.

3.3 Interpretation of the Problem in Terms of Matrices

In free-space solution, each impedance matrix element is obtained from the interaction of a basis and a testing function, or in other words, from the interaction of four triangles. Since testing and basis functions are the same, there is a diagonal symmetry in the impedance matrix:

$$Z_{ij} = Z_{ji}. \tag{3.7}$$

This property is used in order to minimize the computational load. In Chapter 2, two solution methods are explained for the scattering problem of a body above the ground plane. Here, we focus on the relation between the impedance

matrices obtained from these two methods. Assume that we have a square plate on the ground plane. Figures 3.5(a), (b), and (c) show the original problem, the equivalent problem, and the modified triangulated surface respectively. When we apply Eq. (2.12) (free-space Green's function method) to the equivalent problem by replacing $\mathbf{b}_j^{tot}(\mathbf{r}')$ with $\mathbf{b}_j(\mathbf{r}')$, we obtain the equation
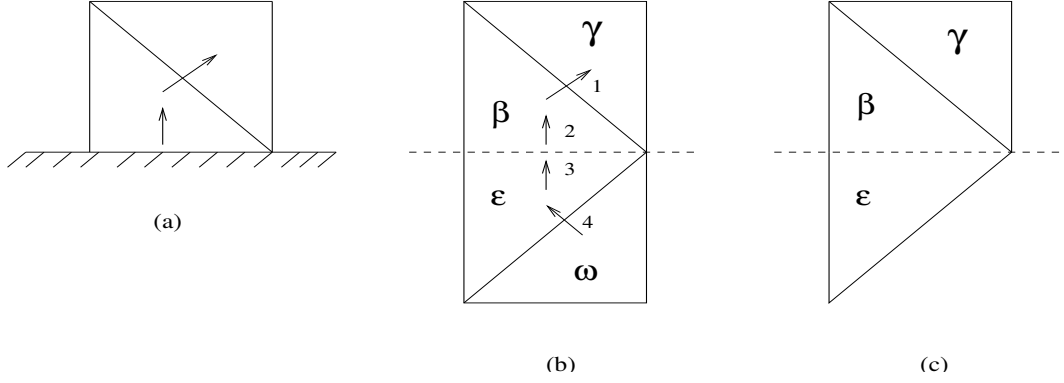

Figure 3.5: (a) A conducting square plate on the ground plane. (b) The equivalent problem. (c) The modified triangulated surface.

$$
\begin{bmatrix}
Z_{11} & Z_{12} & Z_{13} & Z_{14} \\
Z_{21} & Z_{22} & Z_{23} & Z_{24} \\
Z_{31} & Z_{32} & Z_{33} & Z_{34} \\
Z_{41} & Z_{42} & Z_{43} & Z_{44}
\end{bmatrix}
\begin{bmatrix}
\alpha_1 \\
\alpha_2 \\
\alpha_3 \\
\alpha_4
\end{bmatrix}
=
\begin{bmatrix}
V_1 \\
V_2 \\
V_3 \\
V_4
\end{bmatrix}
$$

with the impedance-matrix elements

$$
\begin{aligned}
Z_{11} &= \langle \gamma, \gamma \rangle + \langle \beta, \beta \rangle - 2\langle \gamma, \beta \rangle \\
Z_{12} &= \langle \gamma, \beta \rangle - \langle \beta, \beta \rangle = Z_{21} \\
Z_{13} &= \langle \beta, \varepsilon \rangle - \langle \gamma, \varepsilon \rangle = Z_{31} \\
Z_{14} &= \langle \gamma, \varepsilon \rangle + \langle \beta, \omega \rangle - \langle \gamma, \omega \rangle - \langle \varepsilon, \beta \rangle \\
Z_{22} &= \langle \beta, \beta \rangle \\
Z_{23} &= -\langle \beta, \varepsilon \rangle = Z_{32} \\
Z_{24} &= \langle \beta, \varepsilon \rangle - \langle \beta, \omega \rangle.
\end{aligned}
\tag{3.8}
$$

Actually, some matrix elements are composed of less than four triangle interactions, as will be explained later in this section. Using image theory, we can equate the coefficients of the basis functions as

$$
\begin{aligned}
\alpha_1 &= \alpha_4, \\
\alpha_2 &= \alpha_3.
\end{aligned}
$$
(3.9)

Using the interpretation of the matrix elements in terms of triangles, the size of impedance matrix can be reduced from 4×4 to 2×2 by using the equality between the coefficients:

$$
\begin{bmatrix}
Z_{11} + Z_{14} & Z_{12} + Z_{13} \\
Z_{21} + Z_{24} & Z_{22} + Z_{23}
\end{bmatrix}
\begin{bmatrix}
\alpha_1 \\
\alpha_2
\end{bmatrix}
=
\begin{bmatrix}
V_1 \\
V_2
\end{bmatrix}
$$

It is important to note that the reduced matrix is still symmetric since

$$
\begin{aligned}
Z_{12} + Z_{13} &= \langle \gamma, \beta \rangle - \langle \beta, \beta \rangle + \langle \beta, \varepsilon \rangle - \langle \gamma, \varepsilon \rangle \\[4pt]
&\quad \Updownarrow \qquad \Updownarrow \qquad \Updownarrow \qquad \Updownarrow \\[4pt]
Z_{21} + Z_{24} &= \langle \gamma, \beta \rangle - \langle \beta, \beta \rangle + \langle \beta, \varepsilon \rangle - \langle \beta, \omega \rangle.
\end{aligned}
$$
(3.10)

On the other hand, the method derived in Chapter 2 directly produces the same 2×2 matrix.

In the above, the triangles are denoted by Greek characters, and the interaction of triangles are expressed with inner products. The matrix element Z_{11} is given by

$$
Z_{11} = \int_s ds\, \mathbf{t}_1(\mathbf{r}) \cdot iw\mu \left[\bar{\mathbf{I}} + \tfrac{1}{k^2} \nabla \nabla \right] \cdot \int_{s'} ds'\, g(\mathbf{r}, \mathbf{r}') \mathbf{b}_1(\mathbf{r}').
$$
(3.11)

Both of the integrals are taken on a pair of triangles denoted by γ and β. Then Eq. (3.11) can also be expressed as follows:

$$
\begin{aligned}
Z_{11} &= \underbrace{\int_\gamma ds\, \mathbf{t}_1(\mathbf{r}) \cdot iw\mu \left[\bar{\mathbf{I}} + \tfrac{1}{k^2}\nabla\nabla\right] \cdot \int_\gamma ds'\, g(\mathbf{r},\mathbf{r}')\mathbf{b}_1(\mathbf{r}')}_{\langle \gamma, \gamma \rangle} \\
&+ \underbrace{\int_\beta ds\, \mathbf{t}_1(\mathbf{r}) \cdot iw\mu \left[\bar{\mathbf{I}} + \tfrac{1}{k^2}\nabla\nabla\right] \cdot \int_\beta ds'\, g(\mathbf{r},\mathbf{r}')\mathbf{b}_1(\mathbf{r}')}_{\langle \beta, \beta \rangle} \qquad (3.12) \\
&- 2\underbrace{\int_\gamma ds\, \mathbf{t}_1(\mathbf{r}) \cdot iw\mu \left[\bar{\mathbf{I}} + \tfrac{1}{k^2}\nabla\nabla\right] \cdot \int_\beta ds'\, g(\mathbf{r},\mathbf{r}')\mathbf{b}_1(\mathbf{r}')}_{\langle \gamma, \beta \rangle}.
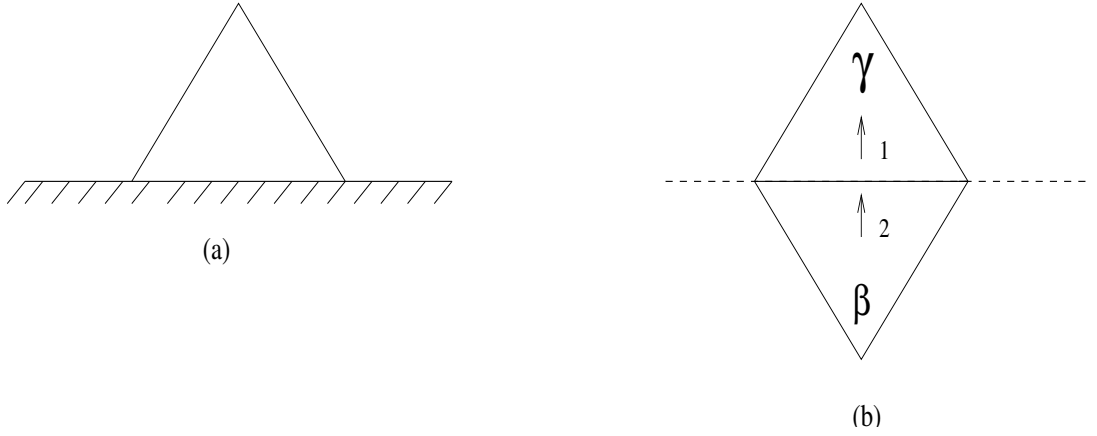\end{aligned}
$$

Figure 3.6: (a) A conducting triangle on the ground plane. (b) The equivalent problem.

Finally, we consider why some matrix elements are composed of less than four triangle interactions. In Figures 3.6 (a) and (b), a single triangle on the ground plane and its equivalent problem are shown. Since one basis function can be defined on these two triangles, the impedance matrix includes only one element:

$$
\begin{bmatrix} Z_{11} \end{bmatrix} \begin{bmatrix} \alpha_1 \end{bmatrix} = \begin{bmatrix} V_1 \end{bmatrix}, \qquad (3.13)
$$

where

$$
Z_{11} = \langle \gamma, \gamma \rangle + \langle \beta, \beta \rangle - 2\langle \gamma, \beta \rangle. \qquad (3.14)
$$

21

The equality between the real and image triangles causes self-interactions ($\langle\gamma,\gamma\rangle = \langle\beta,\beta\rangle$) to be identical. Thus, we can simplify Eq. (3.13) as

$$\left(\langle\gamma,\gamma\rangle - \langle\gamma,\beta\rangle\right)\alpha_1 = \frac{V_1}{2}. \tag{3.15}$$

Consequently, it is possible to solve the problem by evaluating less interactions among the triangles. From the physical point of view, observation point $\mathbf{r}$ should always be on a real triangle, and not on an image triangle in the region below the ground plane. Therefore, the testing process is carried out only on the real part of the body.

Chapter 4

Radiation from a Conducting Body Excited with a Delta-Gap Source

In earlier chapters, the induced current on the body was produced by an incident electromagnetic plane wave, and the scattering problem was considered. In this chapter, we focus on delta-gap source model, which is mainly used to obtain radiation characteristic of conducting bodies. This source type can be thought as an impressed electric field on a limited region of the conducting body. After the triangulation of the surface, we can easily implement a delta-gap source between adjacent triangles by using a feeding voltage as shown in Figure 4.1. On this conducting strip, electric field is zero everywhere except in the gap between the two triangles. Although the excitation type is different for the radiation problems, the formulation derived in Chapter 2 can still be used. Furthermore, the evaluation of the LHS of Eq. (2.12) becomes quite simple when we use a delta-gap voltage source. Assume that the magnitude of the impressed electric

field is given by

$$\mathbf{E}(r) = \hat{n}\frac{V}{\delta}. \tag{4.1}$$

Then, the integration of the electric field with a testing function over the triangular pair covering the gap will be

$$\lim_{\delta \to 0} \int_s ds \, \mathbf{t}_i(\mathbf{r}) \cdot \mathbf{E}(\mathbf{r}) = \lim_{\delta \to 0} \int_{gap} ds \, \mathbf{t}_i(\mathbf{r}) \cdot \mathbf{E}(\mathbf{r}) = \pm \lim_{\delta \to 0} \frac{V}{\delta}\delta\ell_i = \pm V\ell_i. \tag{4.2}$$

Since the electric field and the testing function can be in the same or opposite directions, the result of integration Eq.(4.2) becomes $+V\ell_i$ or $-V\ell_i$.

In this study, we consider two types of implementation of delta-gap sources. One of them is on the connections of triangulated surfaces of the conducting body, the other one is between the ground plane and the conducting body.
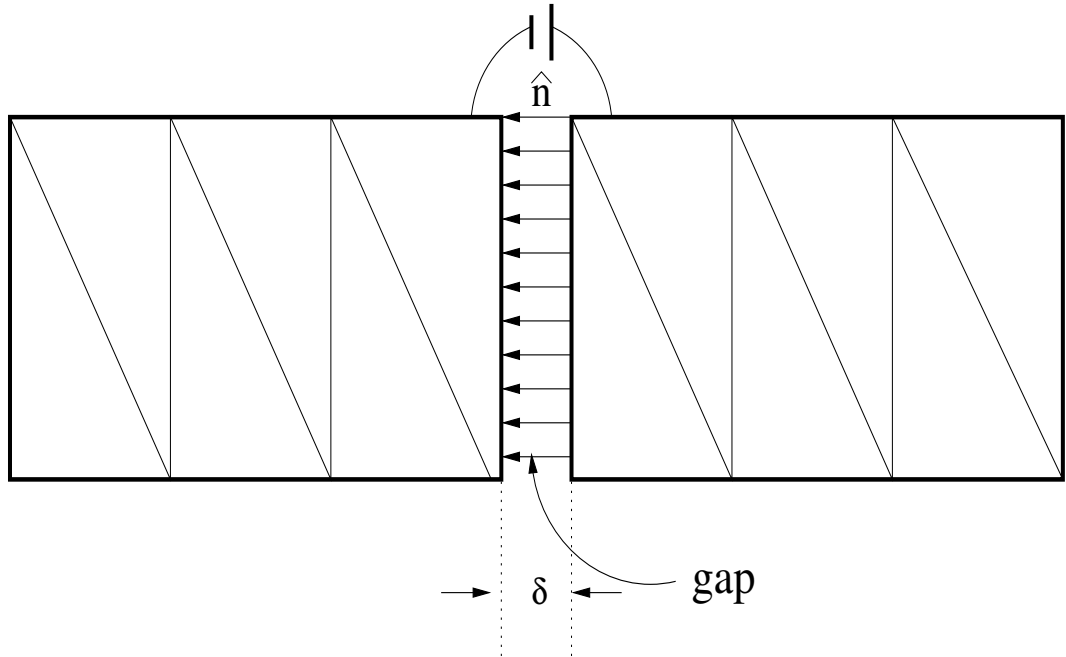

Figure 4.1: Implementation of a delta-gap source between adjacent triangles on a strip.

4.1 Infinitesimal Electric Dipole Above the Ground Plane

In order to construct a dipole for numerical solution, we use a thin conducting strip, whose length is less than 1/10 of the wavelength, excited with a delta-gap source as shown in Figure 4.2(a). Formulation in Chapter 2 can be directly used for the computation of induced currents on this strip. Morever, the analytical solution of the problem illustrated in Figure 4.2(b) is available [7], and is given by

$$
\mathbf{E}_\theta(\mathbf{r}) \simeq
\begin{cases}
j\eta \dfrac{k I_0 l e^{-jkr}}{4\pi r} \sin\theta \big(2\cos(kh\cos\theta)\big) & z \geq 0, \\
0 & z < 0,
\end{cases}
\tag{4.3}
$$

where I_0, l, and h are respectively the magnitude of the current, the length of the dipole, and the height of the dipole from the ground plane. Figure 4.3 presents a comparison of the radiated fields computed by the analytical expression of Eq. (4.3) and the numerical technique. The remarkable agreement of the two sets of data testifies to the accuracy of the numerical solution.
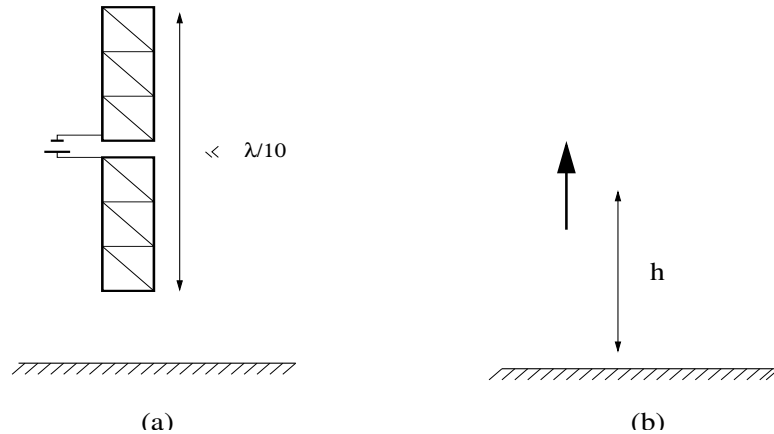

Figure 4.2: (a) A conducting strip approximating an infinitesimal dipole. (b) An infinitesimal electric dipole above the ground plane.
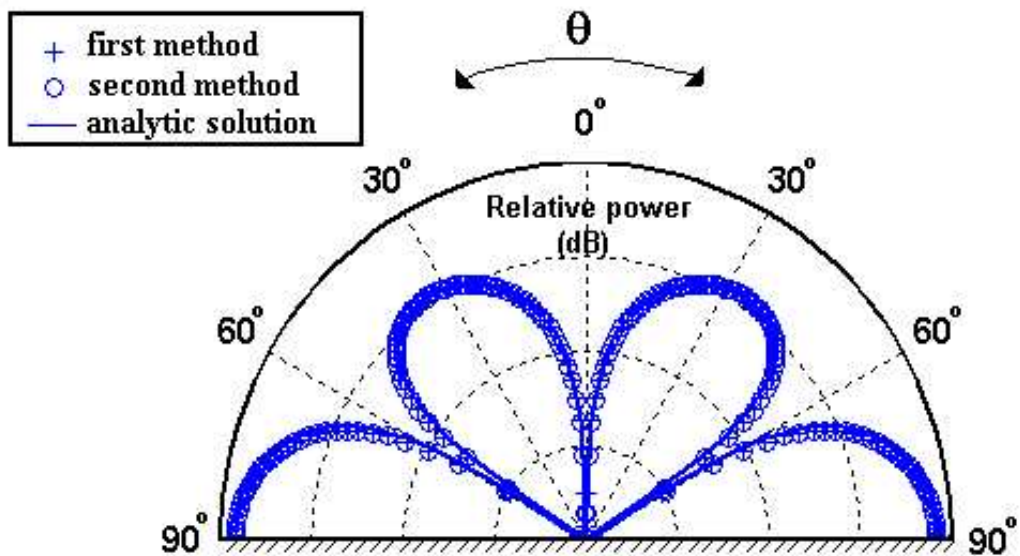
Figure 4.3: Comparison of radiation patterns of a dipole at a height of 0.4585λ above the ground plane.

4.2 A Delta-Gap Source Between Ground Plane and Conducting Body

A delta-gap source can also be defined between the ground plane and the conducting body, as shown in Figure 4.4. In this case, the result of integration in Eq. (4.2) will be exactly the same. However, the result of integration for the equivalent problem will be two times of the original result, since the width of the gap becomes 2δ:
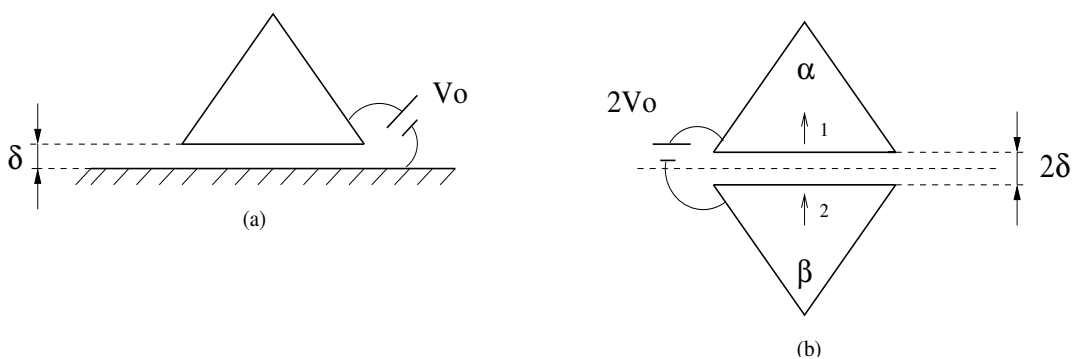

Figure 4.4: (a) Delta-gap source between a single conducting triangle and the ground plane. (b) The equivalent problem.

$$\lim_{\delta \to 0} - \int_s ds \, \mathbf{t}_i(\mathbf{r}) \cdot \mathbf{E}(\mathbf{r}) = \mp 2V\ell_i. \tag{4.4}$$

A quarter-wavelength monopole on a ground plane is equivalent to a half-wavelength dipole in free space, as shown in Figure 4.5. Since the dipole touches the ground plane, we can define a delta-gap source between the ground plane and the dipole as in Figure 4.4. In the example of Section 4.1, the magnitudes of the voltages produced by the impressed electric fields were the same for both the original and the equivalent problems. However, when a delta-gap source is defined between the monopole and the ground plane, the magnitude of the voltage for the equivalent problem is twice the original result, according to Eq. (4.4).
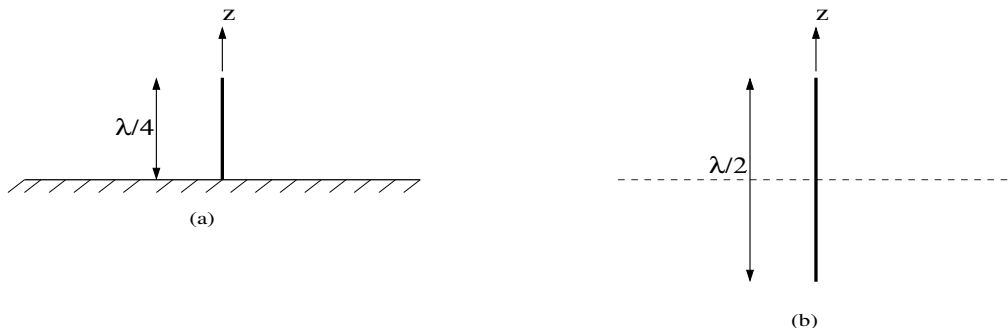

Figure 4.5: (a) A quarter-wavelength monopole on the ground plane. (b) The equivalent problem.

In Figure 4.6, the first method represents the solution of a half-wavelength dipole in free space. In this solution, a delta-gap source is employed at $z = 0$. On the other hand, the second method represents the solution of a monopole in the presence of the ground plane according to the formulation in Chapter 2 by employing a delta-gap source between the monopole and the ground plane.
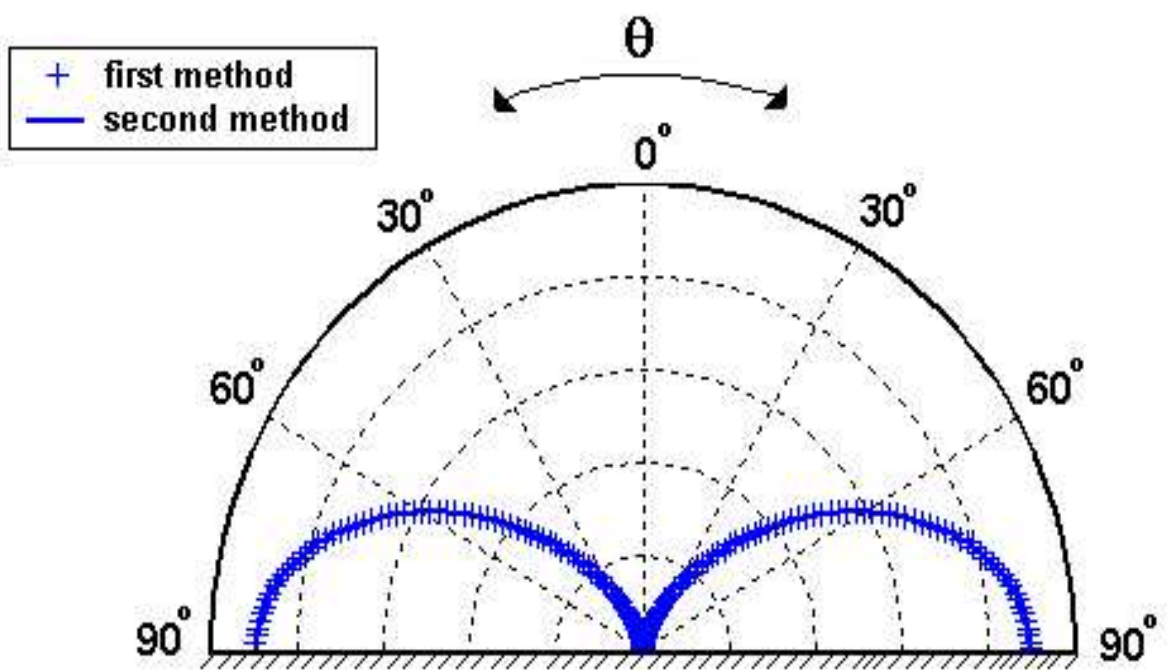
Figure 4.6: Comparison of radiation patterns of the original and the equivalent problems defined in Figure 4.5.

Chapter 5

Multiple Unknowns at a Single Edge

Triangular meshing of some complex geometries may contain cases of more than two triangles connected to the same edge. For this type of edges, multiple basis functions should be defined.

In this work, the cases of three-triangle and four-triangle connections to the same edge are examined. The total numbers of possible basis functions defined are three and six for three-triangle and four-triangle connections, respectively. However, defining all possible basis functions produces linearly dependent equations causing a rank-deficient matrix equation. A methodology used to determine the basis functions to be selected is explained here. Choosing any two of the three possible basis functions is adequate to yield linearly independent equations for the three-triangle connection case. Similarly, choosing three of the six possible basis functions becomes sufficient for the four-triangle connection case. However, there is another constraint regarding the selection of three basis functions. There are twenty different combinations, and in some combinations, all basis functions

are defined on three triangles leaving one triangle empty. These types of combinations give erroneous results since they do not consider the current on one triangle. Therefore, the selected basis functions should cover all of the connected triangles.

5.1   Three-Triangle Connections

Figure 5.1 shows the three possible basis functions on a three-triangle connection. The directions of basis functions can be determined arbitrarily, but all the computations should be consistently carried out by retaining these predetermined directions.
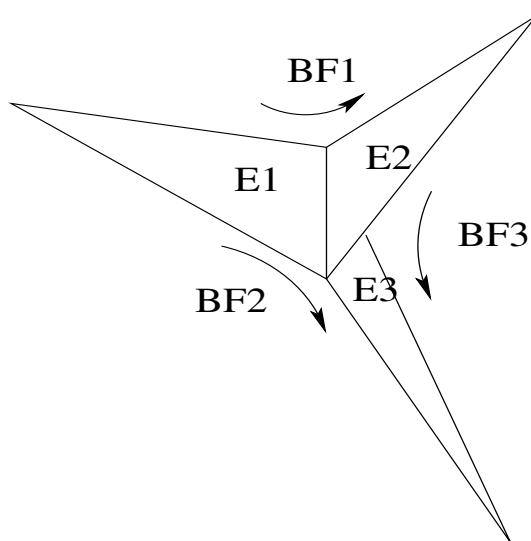

Figure 5.1: Three possible basis functions on a three-triangle connection.

5.1.1   Linear Dependence of Defined Currents

Each element of the impedance matrix is evaluated by considering four triangle-triangle interactions. According to combinations shown in Figure 5.1,

the interpretations of nine matrix elements in the form of triangle-triangle inter-
actions are given by

$$
\begin{aligned}
Z_{11} &= \langle 1,1 \rangle + \langle 2,2 \rangle - 2\langle 1,2 \rangle \\
Z_{12} &= \langle 1,1 \rangle + \langle 2,3 \rangle - \langle 1,3 \rangle - \langle 1,2 \rangle = Z_{21} \\
Z_{13} &= \langle 1,2 \rangle + \langle 2,3 \rangle - \langle 1,3 \rangle - \langle 2,2 \rangle = Z_{31} \\
Z_{22} &= \langle 1,1 \rangle + \langle 3,3 \rangle - 2\langle 1,3 \rangle \\
Z_{23} &= \langle 1,2 \rangle + \langle 3,3 \rangle - \langle 1,3 \rangle - \langle 2,3 \rangle = Z_{32} \\
Z_{33} &= \langle 2,2 \rangle + \langle 3,3 \rangle - 2\langle 2,3 \rangle.
\end{aligned}
\tag{5.1}
$$

Any row of the impedance matrix can be obtained by adding or subtracting the
other two rows. For instance, the elements of the last row can be obtained by
subtracting the first row from the second row:

$$
\begin{aligned}
Z_{31} &= Z_{21} - Z_{11} \\
Z_{32} &= Z_{22} - Z_{12} \\
Z_{33} &= Z_{23} - Z_{13}.
\end{aligned}
\tag{5.2}
$$

Thus, the third row is linearly dependent, and the rank of this 3×3 matrix is
equal to 2. In order to overcome this problem, any two of the three possible basis
functions should be selected for the solution of the matrix equation.

5.1.2   Selection of the Basis Functions

There are three different possible combinations of basis functions, and these
combinations are shown in Figure 5.2. All three basis functions satisfy Kirchhoff's
current law (KCL) individually. Therefore, all three of these combinations should
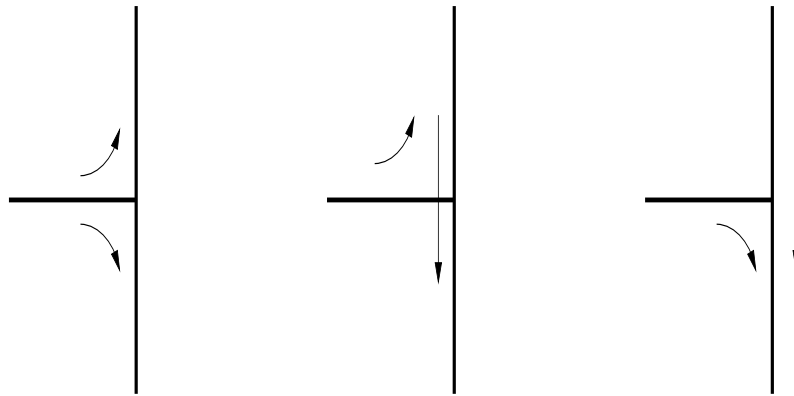produce the same results, such as the overall current distribution and the RCS
values.

Figure 5.2: Three different combinations of basis functions.

As an example, in order to verify that all three choices of the configurations shown in Figure 5.2 produce the same results, we will compare the RCS results obtained for the geometry shown in Figure 5.3. Figure 5.4 shows that the three different RCS results obtained by employing the three different choices of basis-function combinations of Figure 5.2 give exactly the same results.
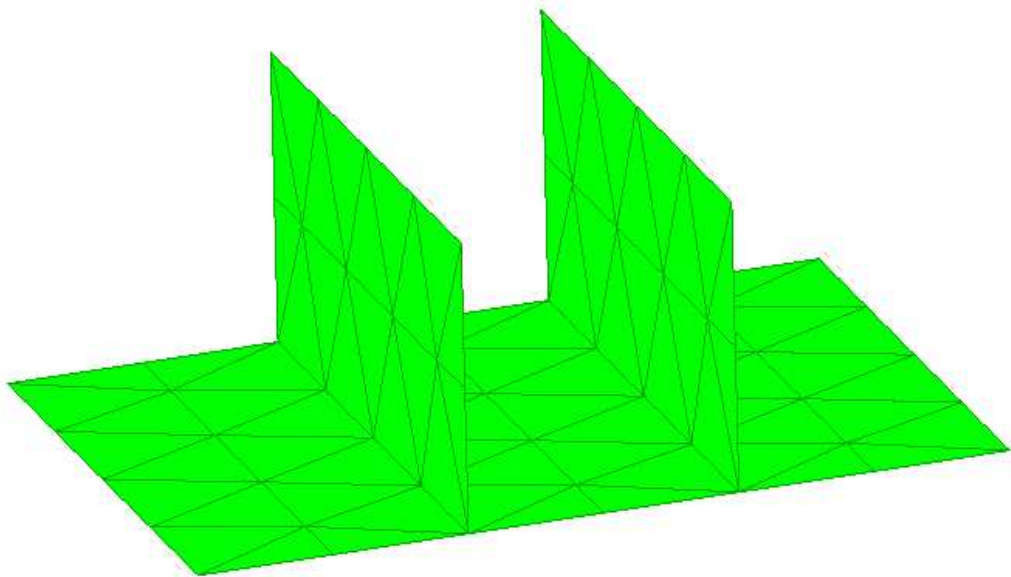

Figure 5.3: A triangulated conducting structure containing three-triangle connections.
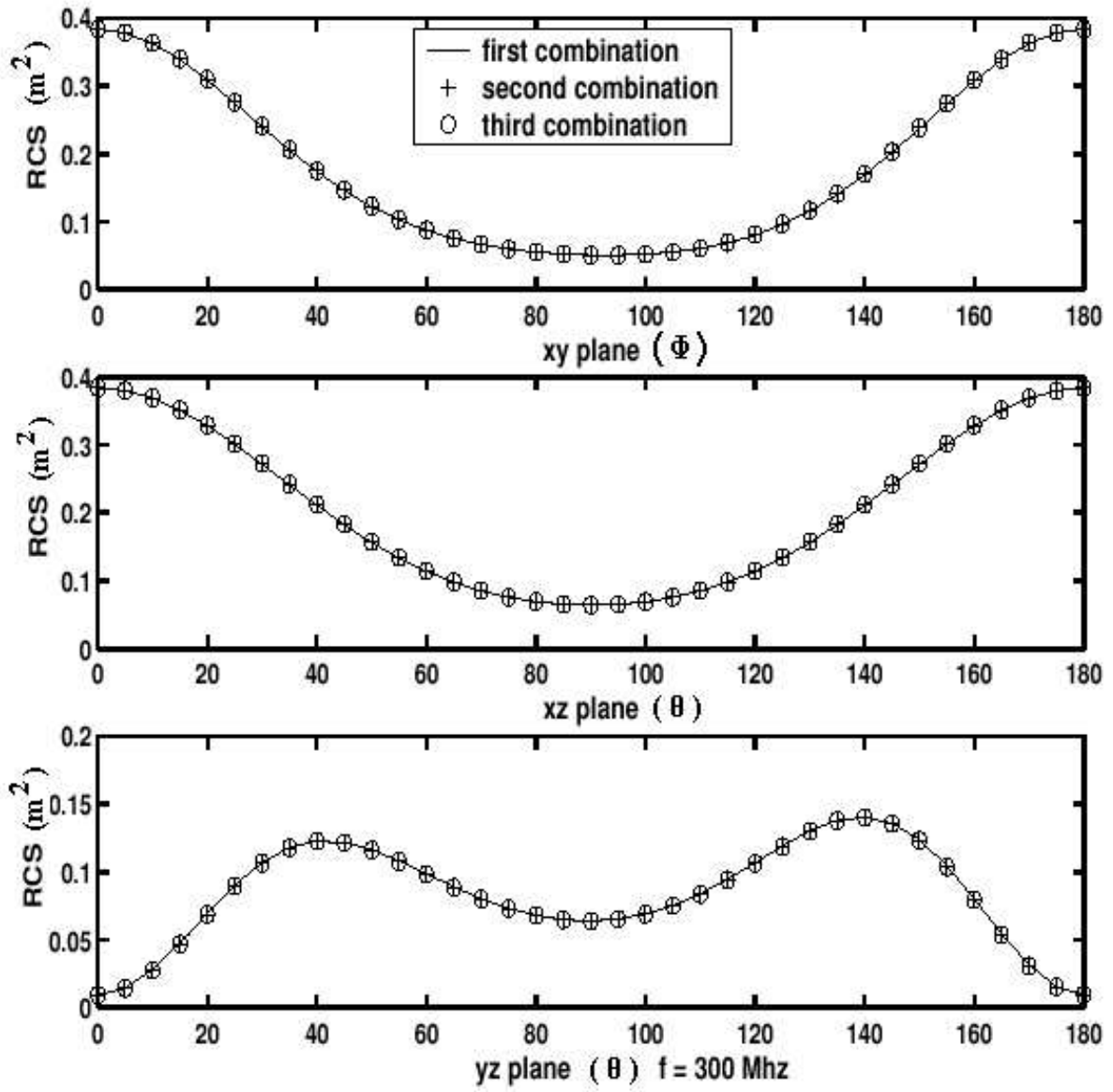
Figure 5.4: The RCS results of the geometry shown in Figure 5.3 using three different combinations of the basis functions.

5.2   Four-Triangle Connections

A similar procedure is applied for the four-triangle connections. There are six possible definitions of current basis functions on four-triangle connections as shown in Figure 5.5. However, three of them are sufficient in order to solve the problem uniquely. The number of all possible combinations of basis functions is equal to 20. However, four of the combinations are not acceptable since they do not cover all four triangles. These invalid combinations are shown in Figure 5.6. Any one of the remaining 16 combinations is valid for a correct formulation of the problem. Figure 5.8 shows the RCS results of the conducting structure whose geometry is presented in Figure 5.7. The legends; "first combination", "second combination", and "third combination" represent different valid combinations of basis functions.
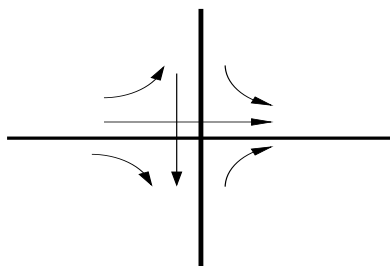

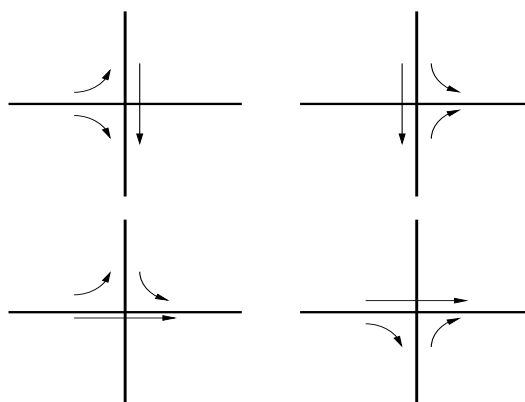Figure 5.5: Six possible basis functions on a four-triangle connection.

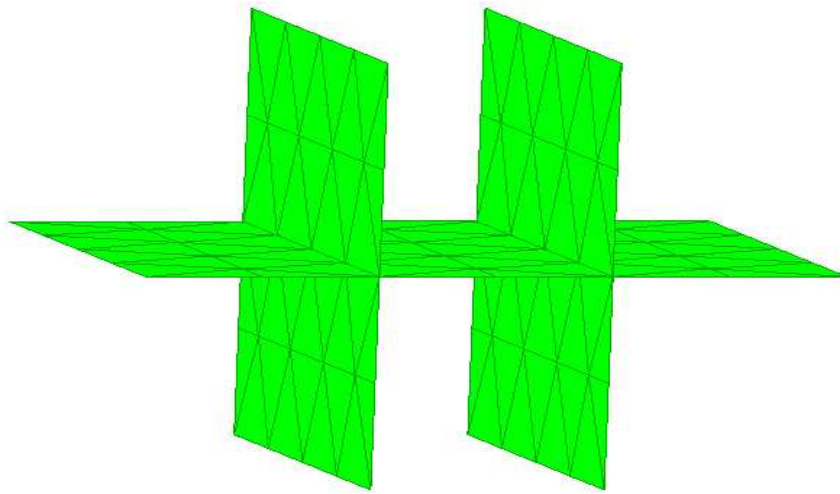Figure 5.6: Four invalid combinations of current basis functions.

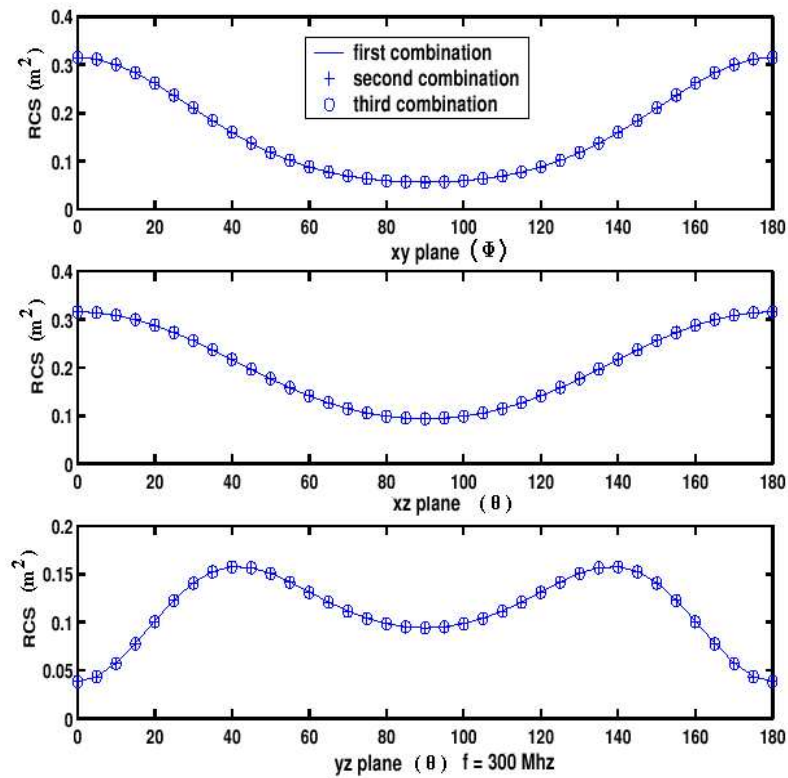Figure 5.7: A triangulated conducting structure having four-triangle connections.

Figure 5.8: The RCS results of the geometry shown in Figure 5.7 using three different combinations from a set of 16 acceptable choices

35

5.3 Delta-Gap Sources on Four-Triangle Connections

Up to three delta-gap sources can be employed on the edges, where four-triangles are connected as in Figure 5.9(a). The solution of problem is performed by using a combination of three valid basis functions. Figure 5.10 shows a triangulated geometry where delta-gap sources are defined at the center, and the radiation patterns of this geometry on three different planes. Three different results are obtained by employing three different valid configurations of the basis functions. The results agree well with each other.

Evaluation of the LHS of Eq. (2.12) for this type of excitation is implemented differently. In the example of Figure 5.9(a), assume that we use the three valid combinations shown in Figure 5.9(b). If we assume that the potential of the delta-gap source is equal to 1, then the normalized entries of the LHS of Eq. (2.12) for the testing functions $1, 2$, and 3 will be $1, 0.5$, and 0.5, respectively. From a physical point of view, the potential difference between the two triangles, where a delta-gap source is defined, is equal to 1, and the potential differences between these two and the remaining triangles are equal to 0.5.
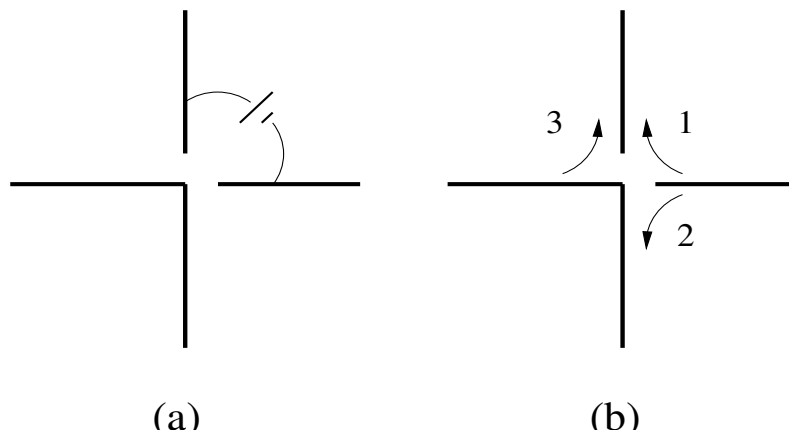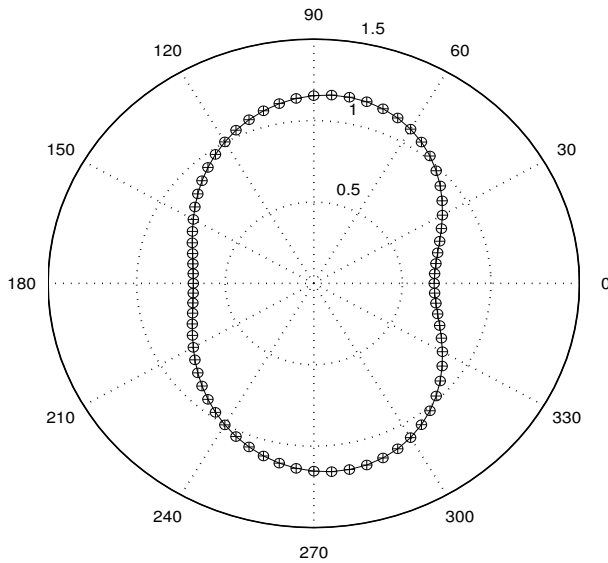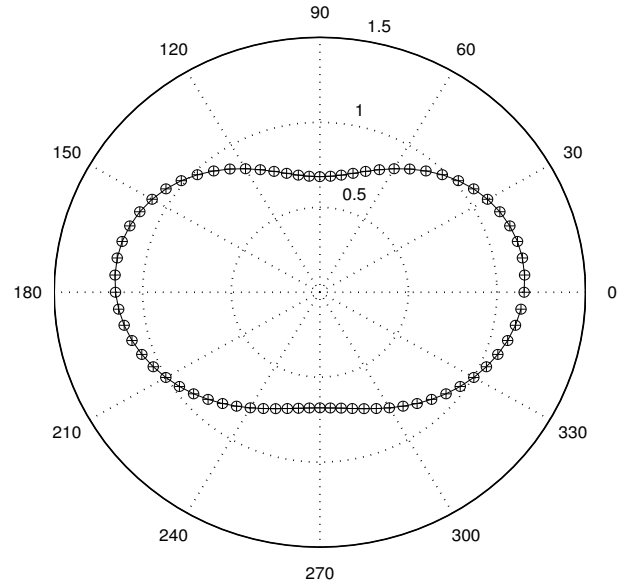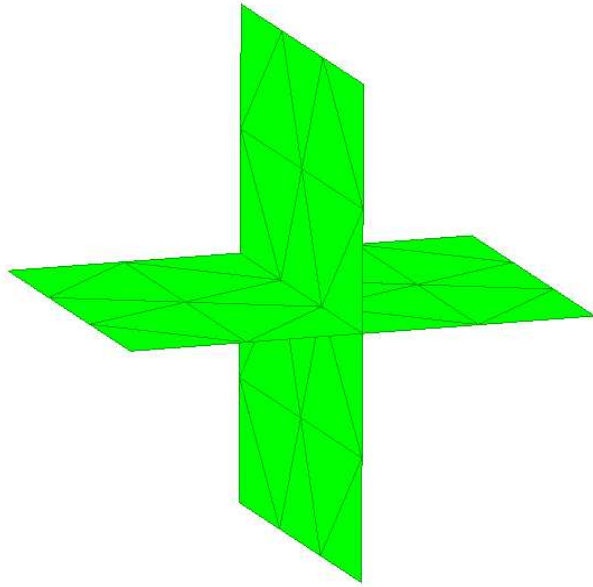

(a)   (b)

Figure 5.9: (a) The implementation of a delta-gap source on a four-triangles connection. (b) One of the valid combinations of basis functions.
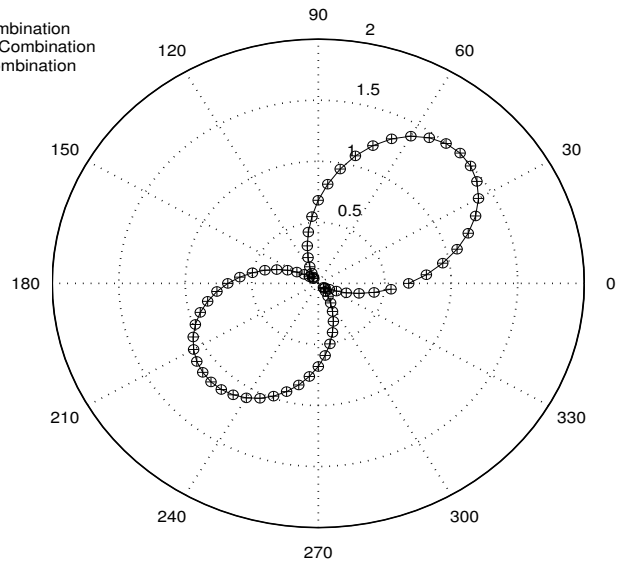
Figure 5.10: A conducting structure containing four-triangle connections and its radiation patterns on three different planes.

5.4 Data Structures for Multiple Connections

After triangulating the surface of the geometry, common edges between the triangles are classified with respect to the number of triangles connected to each edge. In our implementation, two-triangle, three-triangle, and four-triangle connections are considered, and the data comprising the number of triangles connected to the common edges is stored in a matrix. Then, basis functions are defined on connected triangles. The number of basis functions defined is decided according to the number of triangles connected. For the two-triangle case, one basis function is defined on the adjacent triangles, and for the other cases, which are explained in the previous sections of this chapter, two or three basis functions are defined. Two nine-columned connectivity matrices, named CONNECTIVITY1 and CONNECTIVITY2, are used in order to store the defined basis function data. In Table 5.1, filling method of the connectivity matrices is illustrated.

There is no difference between CONNECTIVITY1 and CONNECTIVITY2 matrices in terms of the filling method. However, CONNECTIVITY1 matrix consists of basis functions defined on two-triangle connections, and CONNECTIVITY2 matrix consists of basis functions defined on three-triangle and four-triangle connections. Tables 5.2 and 5.3 show the connectivity matrices of triangulated surfaces shown in Figure 5.11.

Row	1	2	3	4	5	6	7	8	9
T	BF1	BF2	BF3	N1	N2	N3	D1	D2	D3

T : Row index of the CONNECTIVITY matrix, which is also the index
    of the triangular element.

BFi: Indices of the basis functions defined on the three edges of the
     triangle T; 0 if no BF is defined on a particular edge.

Ni: Index of the node across the edge, on which BFi is defined; 0 if no
    BF is defined.

Di: Reference direction of BFi: 1 if BFi is emerging from Ni, 2 if BFi
    is flowing into Ni, 0 if no BF is defined.

Table 5.1: Elements of the CONNECTIVITY matrix.

BF1	BF2	BF3	N1	N2	N3	D1	D2	D3
1	2	0	1	2	0	1	1	0
2	3	0	4	1	0	2	1	0
1	4	0	3	2	0	2	1	0
3	4	0	3	4	0	2	2	0

Table 5.2: CONNECTIVITY1 matrix of triangulated surface shown in Figure 5.11(a).

BF1	BF2	BF3	N1	N2	N3	D1	D2	D3
1	2	3	3	3	3	1	1	1
1	0	0	4	0	0	2	0	0
2	0	0	5	0	0	2	0	0
3	0	0	6	0	0	2	0	0

Table 5.3: CONNECTIVITY2 matrix of triangulated surface shown in Figure 5.11(b).
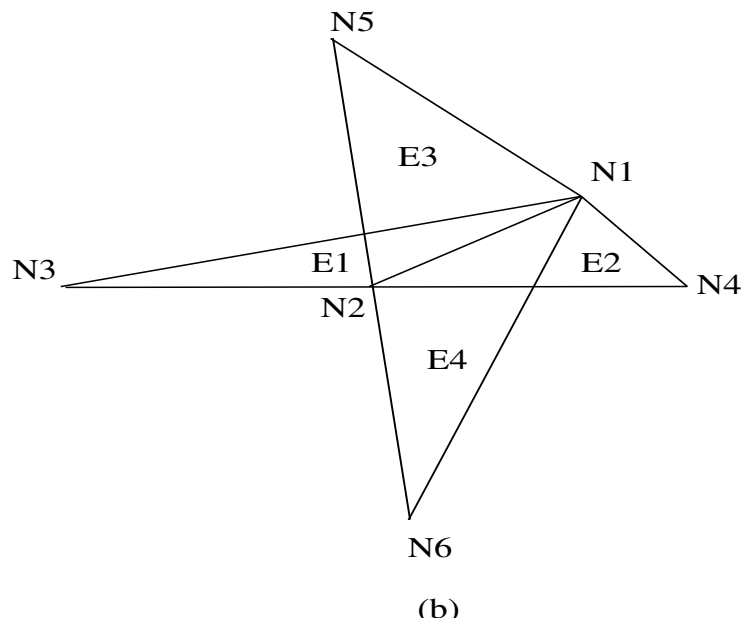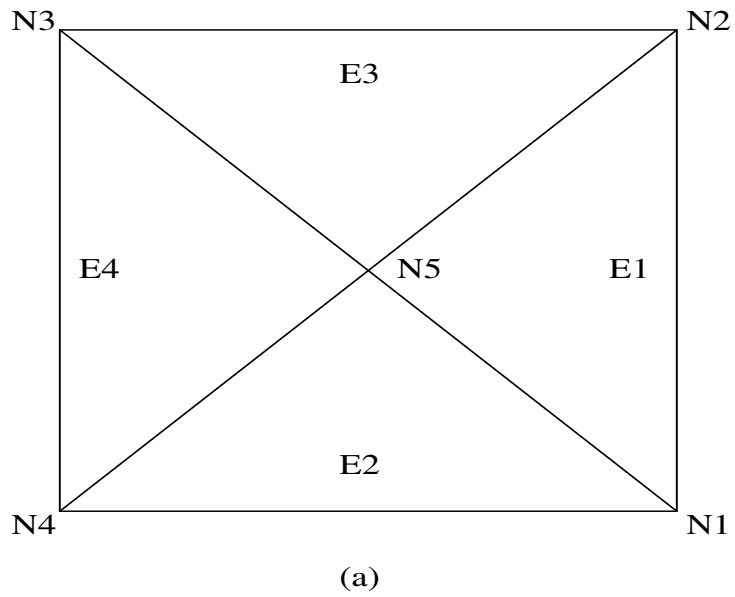
Figure 5.11: (a) A triangulated surface having only two-triangle connections. (b) A triangulated surface having four-triangle connections.

5.5 Scattering from a Complicated Target with Multiple Connections

Formulation and solution of scattering problems in the presence of a ground plane were illustrated in Chapter 2. However, those geometries used did not contain any multiple connections. Although multiple connections complicates the problem in terms of the definitions of the basis functions, solution of the scattering problems involving geometries with multiple connections is exactly the same as in Chapter 2. Figure 5.13 shows the monostatic RCS results, which means that the receiver and the source are in the same location, obtained by employing a ship model, geometry of which is shown in Figure 5.12.

In this problem a y-polarized incident field is used for excitation. Since the y-axis is parallel to the ground plane, it can also be called the horizontal polarization. Furthermore, the equivalent problem is solved by using the geometry in Figure 5.14. The consistency of the results in Figure 5.13 verifies the formulation in Chapter 2. Although the latter method seems straightforward, it produces redundantly large matrix equations. For instance, the first method produces a matrix equation with 959 unknowns, compared to 2145 unknowns of the second method. As the number of unknowns increases, the second method becomes prohibitively expensive compared to the first one.
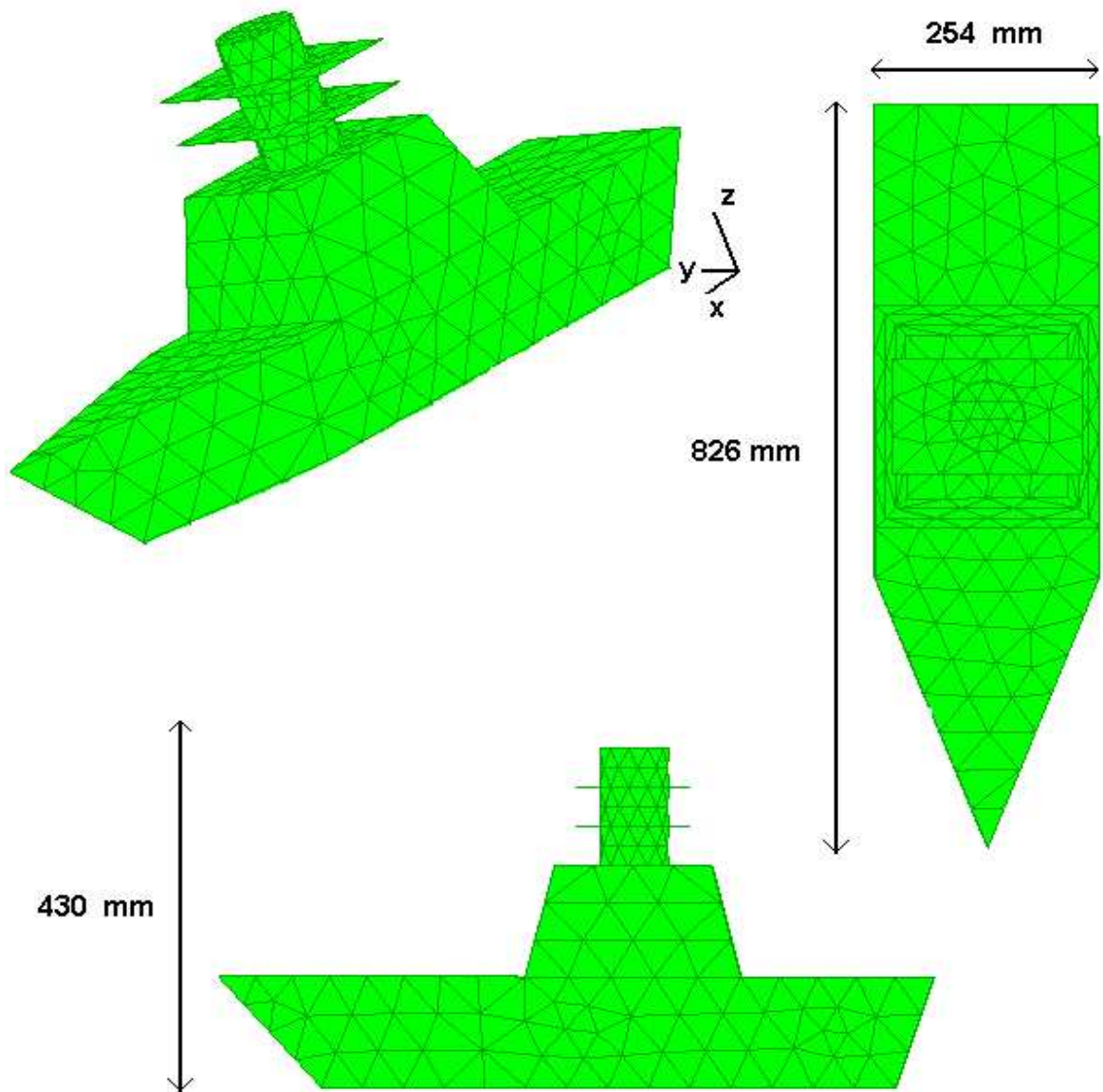
Figure 5.12: A ship model having three-triangle connections.
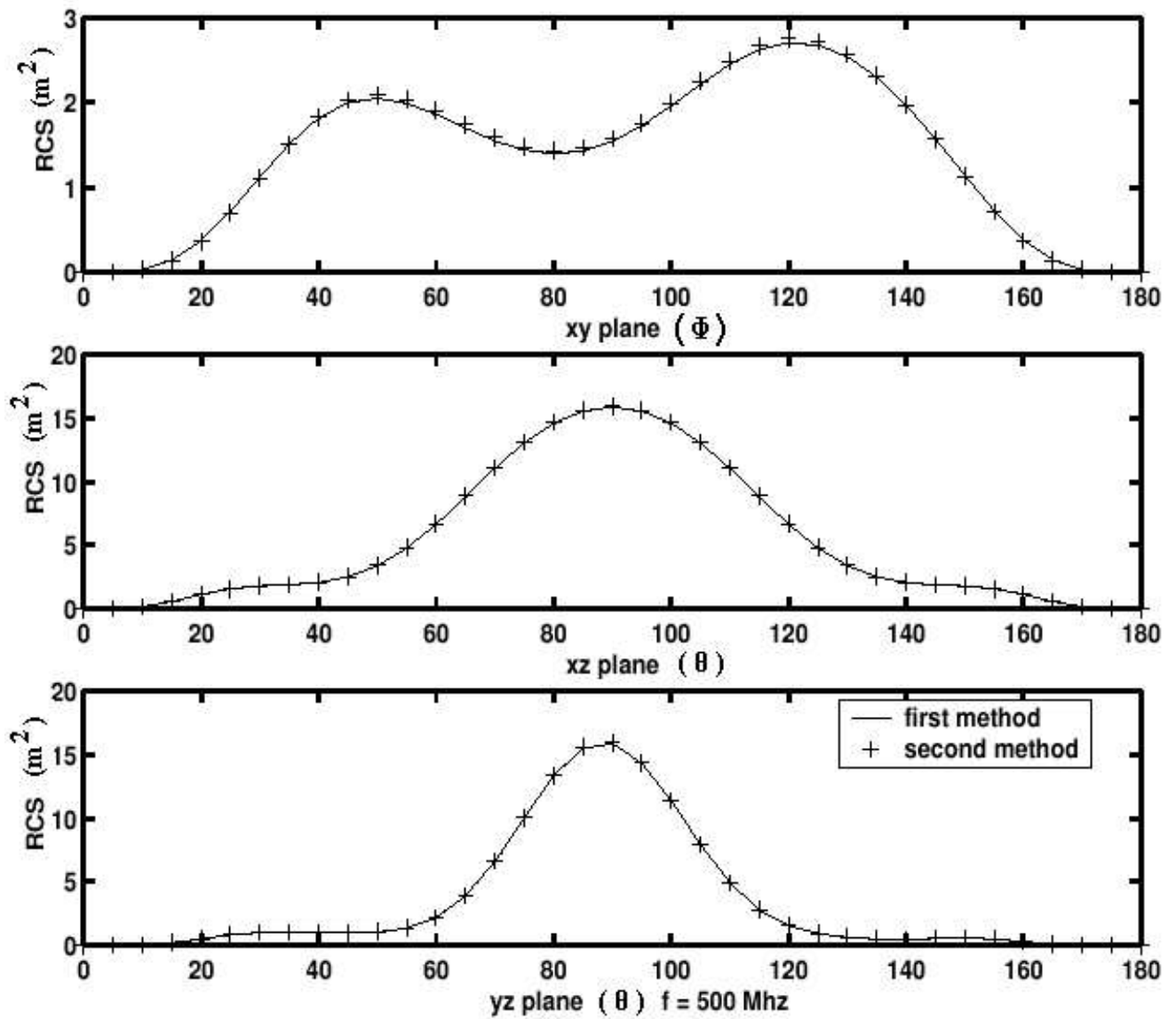
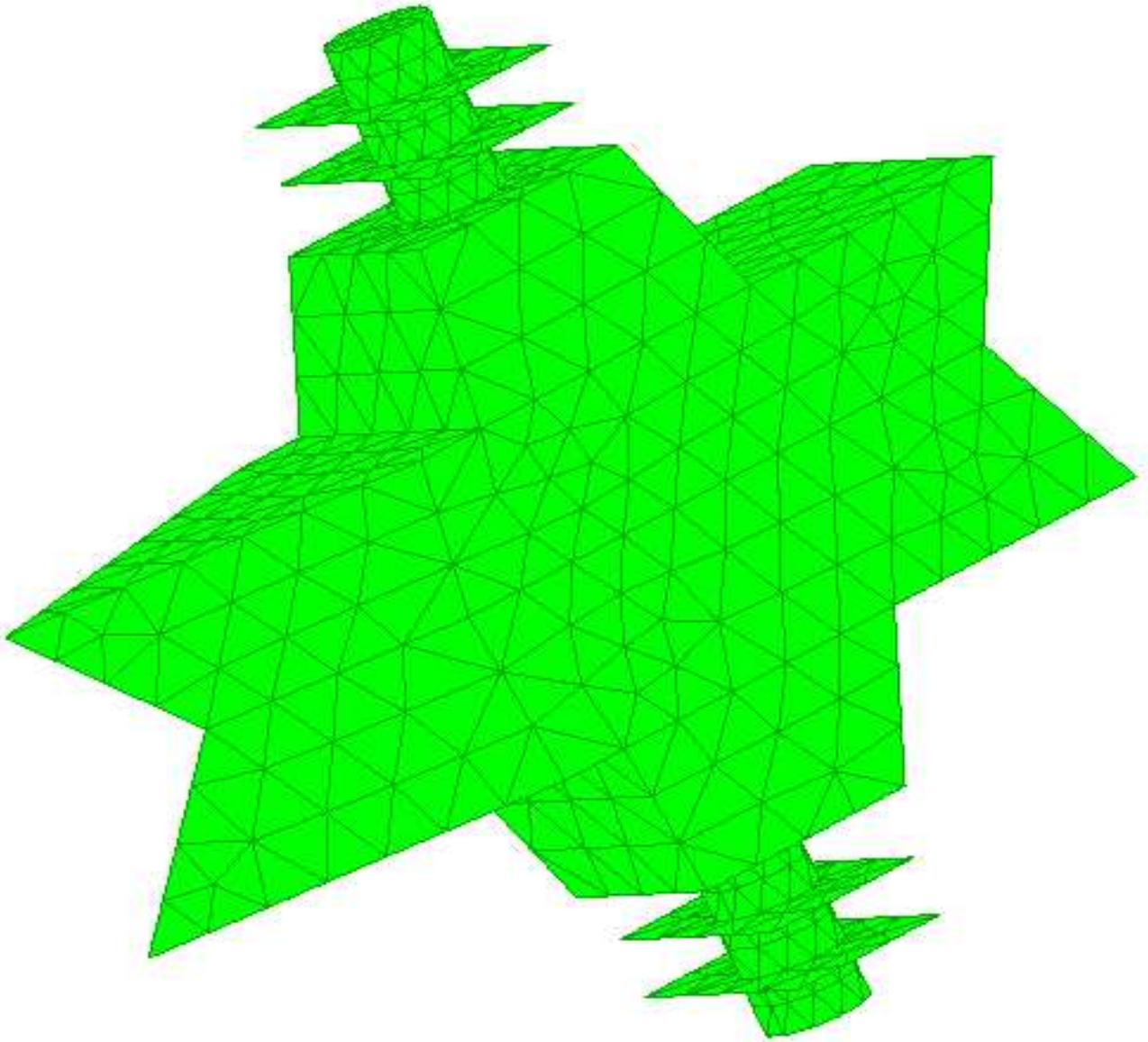Figure 5.13: The monostatic RCS results of ship model shown in Figure 5.12.

Figure 5.14: The geometry of the equivalent problem, used in the second method.

Chapter 6

Conclusions

In this thesis, method of moments in conjunction with the image theory is applied to analyze the electromagnetic scattering from arbitrarily shaped conducting bodies above the ground plane. Two solution methods are presented with their formulations. A special attention is given for the formulation of the second method, which concentrates on the modification of the free-space Green's function. We obtain same numerical results using both of these two methods. Both scattering and radiation phenomena are considered by using two different excitation types.

Complex bodies consisting of multiple connections at single edges are examined. A methodology applied for the definition of the basis functions on these types of edges is developed, and its accuracy is verified by using different valid combinations of basis functions.

As a future work, the same problem can be solved in the presence of a coating over the conducting body. In this case, a MoM solution based on impedance boundary condition (IBC) can be applied for the solution of the problem.

Bibliography

[1] P. Y. Ufimtsev, *Comments on Diffraction Principles and Limitations of RCS Reduction Techniques*, Proc. IEEE, vol. 84, pp. 1828-1851, Dec. 1996.

[2] R. F. Harrington, *Field Computation by Moment Methods.* IEEE Press, Piscataway, NJ, c1993.

[3] E. Arvas, R. F. Harrington, and J. R. Mautz, *Radiation and Scattering from Electrically Small Conducting Bodies of Arbitrary Shape above an Infinite Ground Plane*, IEEE Trans. Antennas Propagat., vol. AP-35, pp. 378-383, Apr. 1987.

[4] S. M. Rao, D. R. Wilton, and A. W. Glisson *Electromagnetic Scattering by Surfaces of Arbitrary Shape*, IEEE Trans. Antennas Propagat., vol. AP-30, pp. 409-418, May 1982.

[5] D. R. Wilton, S. M. Rao, A. W. Glisson, D. H. Schaubert, O. M. Al-Bundak, and C. M. Butler, *Potential Integrals for Uniform and Linear Source Distributions on Polygonal and Polyhedral Domains,* IEEE Trans. Antennas Propagat., vol. AP-32, pp. 276-281, Mar. 1984.

[6] R. D. Graglia, *On the Numerical Integration of the Linear Shape Functions Times the 3-D Green's Function or its Gradient on a Plane Triangle* IEEE Trans. Antennas Propagat. vol. 41, pp. 1448-1455, Oct. 1993.

[7] C. A. Balanis, *Advanced Engineering Electromagnetics.*, John Wiley& Sons, New York, 1989.